# DFO Tanker Safety 2017 Project Report

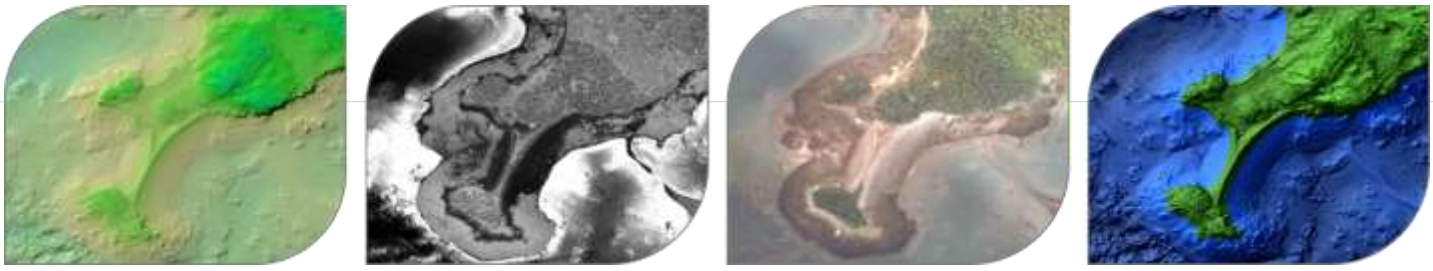


*Prepared by*

Applied Geomatics Research Group
NSCC, Middleton
Tel. 902 825 5475
email: tim.webster@nscc.ca

*Submitted to:*

Fisheries and Oceans Canada
Pêches et Océans Canada

Scott Coffen-Smout
Oceans and Coastal Management Division
Ecosystem Management Branch


May 31, 2017

How to cite this work and report:

Webster, T. 2017. “DFO Tanker Safety 2017 Project Report” Technical report, Applied Geomatics Research Group, NSCC Middleton, NS.

## Executive Summary

Topographic-bathymetric lidar surveys were flown to collect high-resolution seamless land-sea elevation and image data of the land coastal areas at four Nova Scotia and New Brunswick study areas in 2016. The surveyed areas were Deer Island and Grand Manan, islands located in the Bay of Fundy, as well as two Atlantic Ocean study areas, Big Basin and Canso. The sensor used was AGRG's Chiroptera II integrated topographic-bathymetric lidar sensor, equipped with a 60-megapixel multispectral camera.

The objective of this project was to use the derived lidar products (high-resolution bathymetry, laser intensity, aerial photographs, and ground truth data) to support oil spill preparedness in partnership with the Government of Canada's World-Class Tanker Safety Program. The lidar surveys were successful in penetrating to the seabed in each of the areas: in Big Basin, the lidar reached minimum elevation values of -4.94 m CGVD28 (~ MSL), however, it was not successful in penetrating to the center of the Basin due to deep bathymetry and poor water clarity; in Canso, minimum elevation values were -14.91 m CGVD28; in Deer Island, minimum elevation values were -13.17 m CGVD28; and in Grand Manan, minimum elevation values were -11.35 m CGVD28.

Hydrodynamic (HD) models were developed for Canso and Big Basin. Big Basin was combined with Isle Madame surveys from 2014 and 2015 to cover a larger area with high resolution lidar; these models were designed to be larger than the lidar study areas in order to properly model circulation within the Chedabucto Bay into the study areas. The models provide examples of travel time of spilled contaminants and near-shore current speeds to assist with cleanup strategies. AGRG researchers collected survey grade GPS points on roads and wharves within the Grand Manan study area, and were on the water collecting GPS data in Canso and Big Basin, as well as measuring other components including water clarity, depth, and underwater photos of the seabed conditions and bottom type.

Ground truth maps overlaid with the orthophoto mosaic illustrate a cover type of mainly mud in Big Basin with some eelgrass, and sand in Canso, with a mixture of eelgrass and fucus. A shoreline classification of Grand Manan resulted in a primary cover type of submerged dense vegetation and bedrock utilizing the aerial photography data. Bottom classification maps were derived for Big Basin, Canso, and Grand Manan using the lidar and QA orthophotos. Submerged Aquatic Vegetation (SAV) maps were also derived for Big Basin, Canso, and Grand Manan, however, the true colour aerial photograph orthomosaics were used in that classification method.

A Seabird 25plus Conductivity Temperature Depth (CTD) sensor was used during the lidar survey on July 20 at Canso to measure changes in salinity, temperature, turbidity, and chlorophyll through the water column. The CTD data also provided an additional depth validation method. The information on water movement, bottom type, and water depth provided by this project will allow DFO to characterize the estuaries, ensure safe navigation of tankers into the ports, and to better manage response time and logistics in the event of a spill.

# Table of Contents

# Table of Figures

## List of Tables

# 1 Introduction

## 1.1 Project Background

The Government of Canada established the World-Class Tanker Safety program to strengthen Canada's current tanker safety program by preventing oil spills and improving response and cleanup (Government of Canada, 2016). Spill-response planning partnerships were developed as part of the program for several high-traffic ports including Saint John, New Brunswick (NB) and Port Hawkesbury, Nova Scotia (NS). The Area Response Planning Project is a regional, risk-based planning approach that reflects local environmental sensitivities and marine activity; the project aims to establish a new level of oil spill preparedness and response capacity to match the level of regional risk (Government of Canada, 2012).

Nova Scotia Community College's Applied Geomatics Research Group (NSCC-AGRG) is participating in the Atlantic component of the project by surveying several areas in the Atlantic Ocean and Bay of Fundy using an airborne topographic-bathymetric lidar sensor and high-resolution aerial camera. NSCC has recently acquired this sensor, which offers a unique method to survey the shoreline in more detail than present, map and characterize environmentally sensitive areas, use the nearshore bathymetry to model the local tidal currents, and chart nearshore hazards for navigation.

In the summer of 2016, AGRG used the lidar system to survey four areas: two in the Bay of Fundy near the Gulf of Maine and two in the Strait of Canso near the Port Hawkesbury terminal (Figure 1.1.1). This report will highlight the results of the surveys, as well as the derived data products: the digital elevation models, digital surface models and lidar intensity models, all derived from the lidar point cloud. Additionally, this report will present the high-resolution aerial imagery, which is processed using the aircraft trajectory and direct georeferencing. Ground truth maps will highlight the results of the ground truth surveys, such as bottom type and water clarity.

Over the course of this project, AGRG will use these data to generate high-resolution near-shore bathymetry maps, derive substrate and vegetation habitat types, and develop coastal hydrodynamic models. The results of the project will be used as part of the World-Class Tanker Safety program to ensure safe navigation of tankers into the port, and to better manage response time and logistics.

## 1.2 Study Area

The two study areas located on the New Brunswick shoreline of the Bay of Fundy are Deer Island and Grand Manan Island (Figure 1.1). The most northern study area, Deer Island, encompasses several small islands and coves, as well as part of the Deer Island ferry route. Grand Manan Island is the largest of the islands in the Bay of Fundy, requiring several individual surveys to cover the study area. The two Atlantic Ocean study areas are Big Basin and Canso (Figure 1.1). Big Basin, located in Richmond County, is located northwest of Isle Madame and has a river draining into its basin. Canso, located in Guysborough County, is exposed to the ocean and has a series of very small islands dispersed throughout the study area.

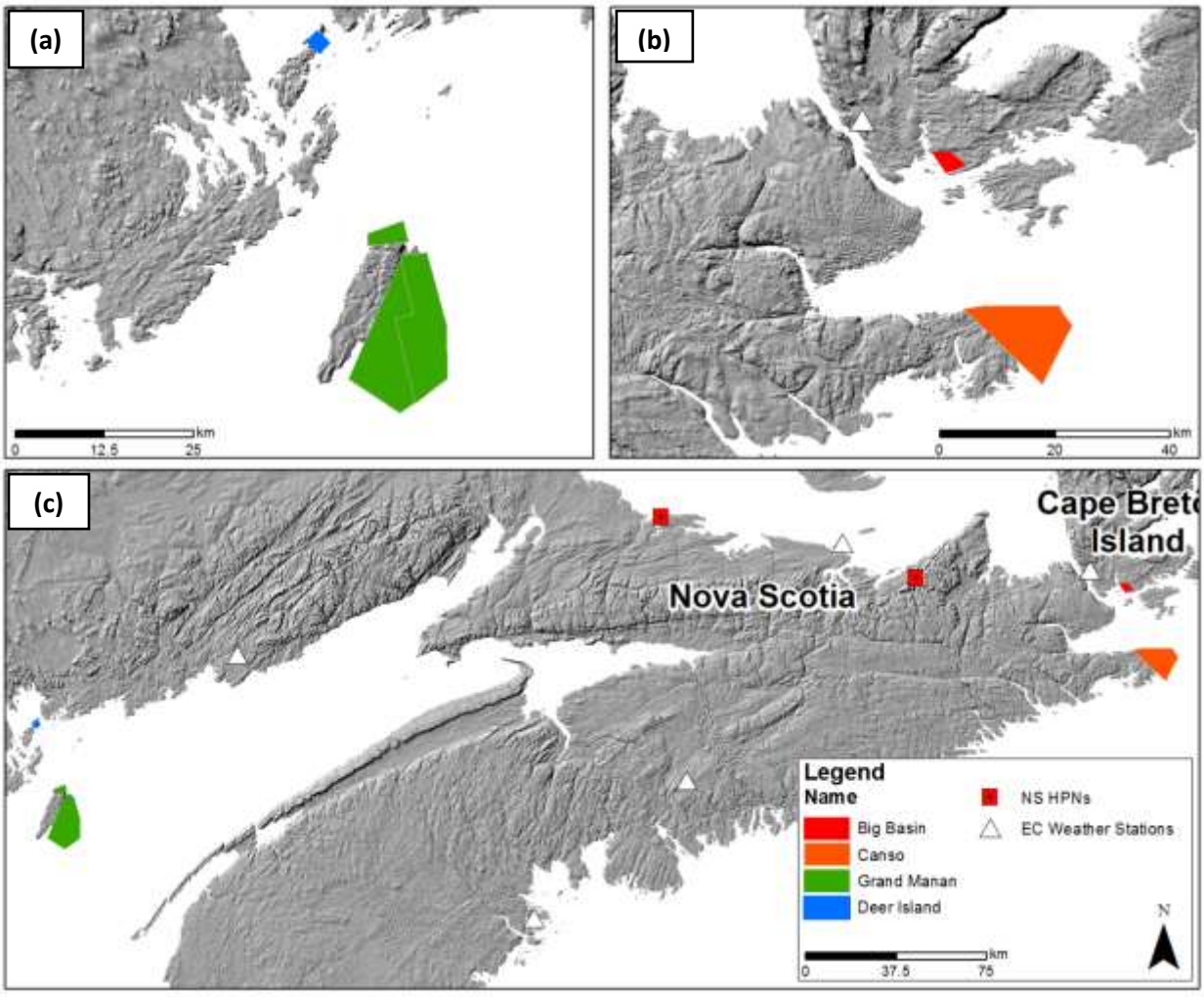


**Figure 1.1: The four topographic-bathymetric lidar study areas surveyed in 2016 (c), the areas in the Bay of Fundy (a), and the two Atlantic Ocean study areas (b). Map also shows NS High Precision Network (HPN) stations (red squares) and Environment Canada (EC) Weather Stations (white triangles).**

# 2 Methods

## 2.1 Sensor Specifications

The lidar sensor used in this study is a Chiroptera II integrated topographic-bathymetric lidar sensor equipped with a 60-megapixel multispectral camera. The system incorporates a 1064 nm near-infrared laser for ground returns and sea surface and a green 515 nm laser for bathymetric returns (Figure 2.1, Figure 2.2d). The lasers scan in an elliptical pattern, which enables coverage from many different angles on vertical faces, causes less shadow effects in the data, and is less sensitive to wave interaction. Water depth and clarity limited bathymetric laser penetration resulting in a depth penetration rating of roughly 1.5 x the Secchi depth (a measure of turbidity or water clarity using a black and white disk). The Leica RCD30 camera (Figure 2.2d) collects co-aligned RGB+NIR motion compensated photographs. Photographs are mosaicked into a single image in post-processing or analyzed frame by frame for maximum information extraction.

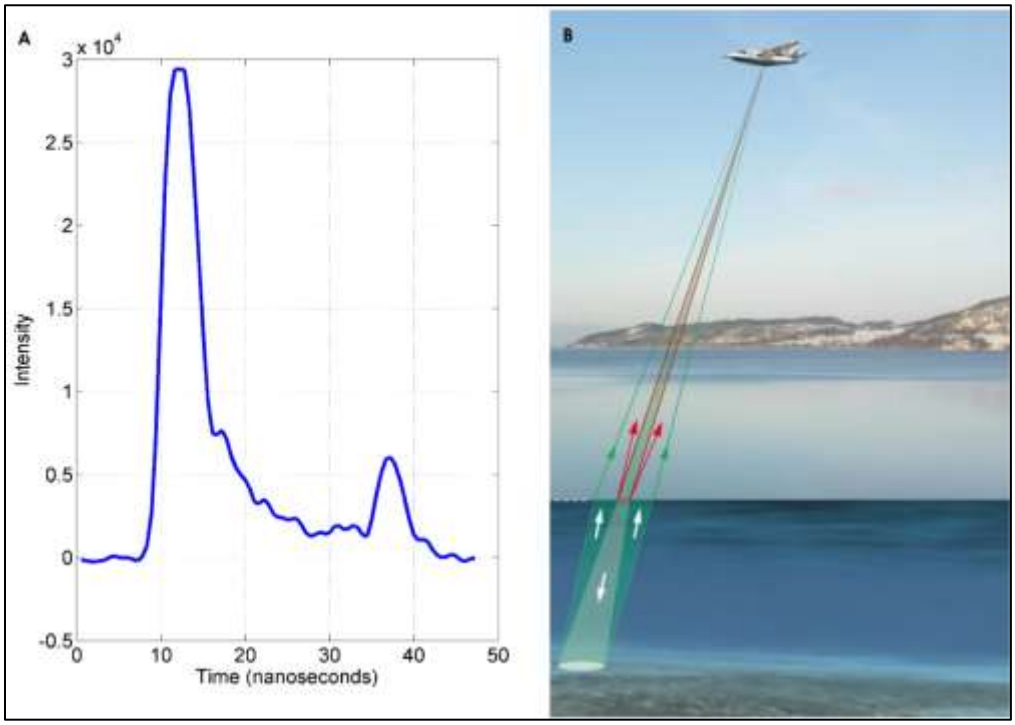


**Figure 2.1: (A) Example of the Chiroptera II green laser waveform showing the large return from the sea surface and smaller return from the seabed. (B) Schematic of the Chiroptera II green and NIR lasers interaction with the sea surface and seabed (adapted from Leica Geosystems).**


**Figure 2.2: (a) Aircraft used for 2016 lidar survey; (b) display seen by lidar operator in-flight; (c) main body of sensor (right) and the data rack(left); (d) large red circles are the lasers; the RCD30 lens (right) and low resolution camera quality control(left).**

## 2.2 Lidar Survey Details

The lidar surveys were conducted in July and August of 2016 (
Table 2.1). The surveys were planned using Mission Pro software. The planned flight lines for each study area are shown in Figure 2.3. The aircraft required ground-based high precision GPS data to be collected during the lidar surveys in order to provide accurate positional data for the aircraft trajectory. Our Leica GS14 RTK GPS system was used to set up a base station set to log observations at 1-second intervals over a Nova Scotia High Precision Network (HPN) (Figure 1.1).

Deer Island was surveyed on July 6, 2016. With 11 flight lines, this was the smallest of the study areas surveyed for this project. Grand Manan Island, the largest of the Fundy islands was also the largest of the Tanker Safety study areas, as indicated in
Table 2.1. 56 flight lines were flown. The Grand Manan survey began on Aug 28 at high tide and ended on a low tide. The remaining Grand Manan surveys were completed on September 17 and 26 respectively, resulting in an almost complete coverage of the southeastern portion of Grand Manan

(Figure 2.4). The Big Basin survey began on July 12 and was completed on July 19. The first survey was flown at a falling tide, while the second was flown at a rising tide. In total, 17 flight lines were surveyed. Finally, Canso was flown on July 20 while AGRG researchers conducted time of flight ground truth surveying (this will be discussed further in Section 2.3). Canso was one of the larger study areas surveyed for this project with 58 flight lines, and presented a challenge with the aerial photography in particular, as the sun was setting during the second half of the survey.

| Study Area | Abbreviated Name | Survey Date | Number of Flight Lines | Area ($km^2$) |
|---|---|---|---|---|
| Deer Island | DI | Jul 06 2016 | 11 | 5.0 |
| Grand Manan | GM | Aug 28, Sept 17, Sept 26 2016 | 56 | 179.5 |
| Big Basin | BB | Jul 12, Jul 19 2016 | 17 | 12.3 |
| Canso | CANSO | Jul 20 2016 | 58 | 95.7 |

**Table 2.1: 2016 Tanker Safety lidar survey dates, durations, areas and flight lines.**

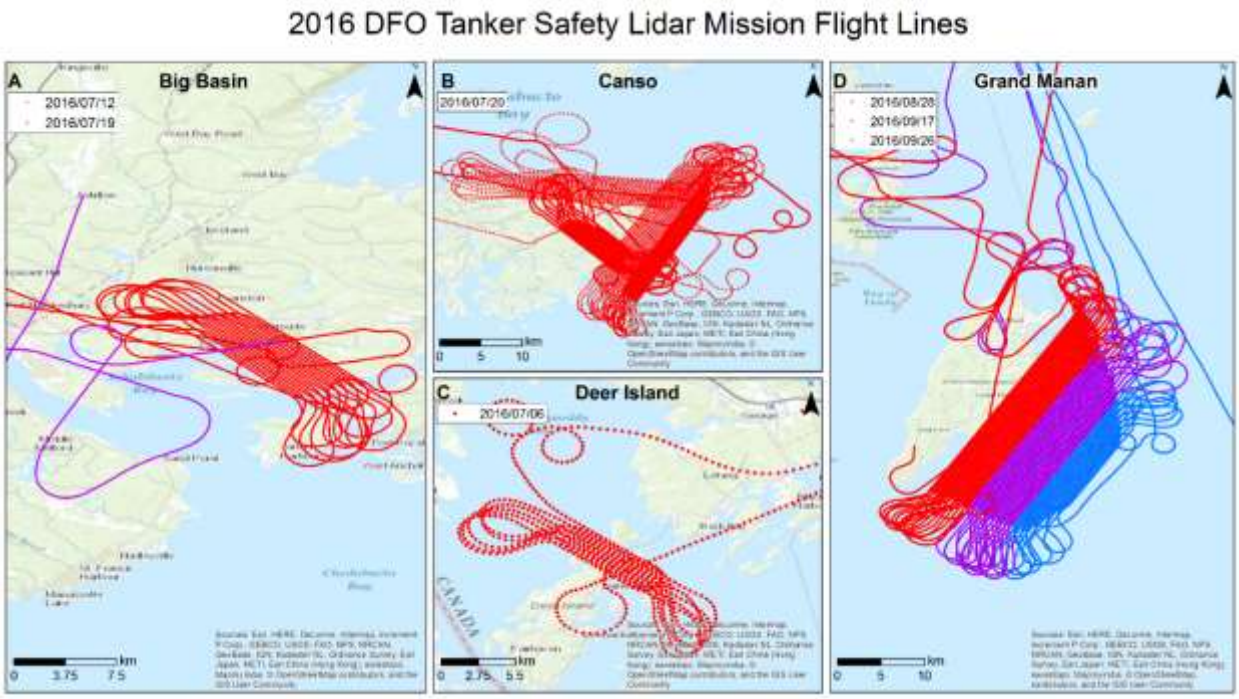

**Figure 2.3: Flight lines for 2016 Tanker Safety study areas.**

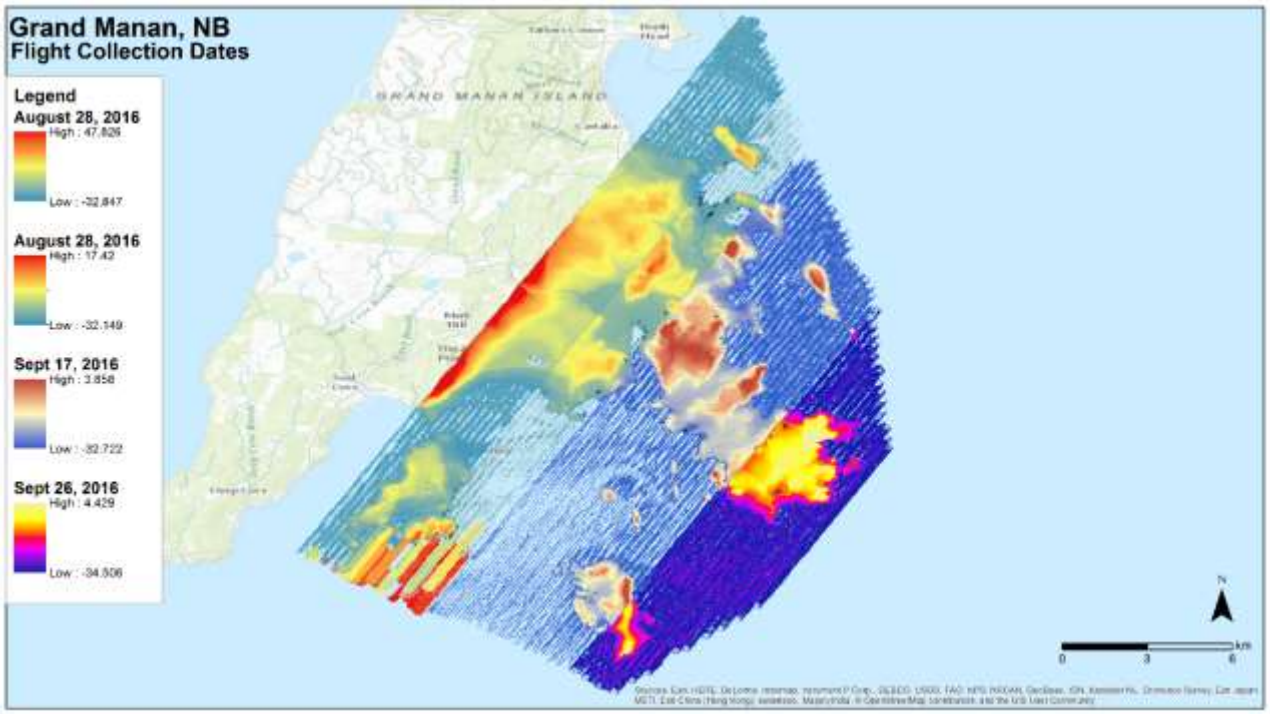


**Figure 2.4: Grand Manan survey flights and coverage from August 28 through September 26, 2016.**

During the Canso collection, an erroneous setting was used during the survey which caused too many points to be collected resulting in 'noisy' topographic-laser data (Figure 2.5).

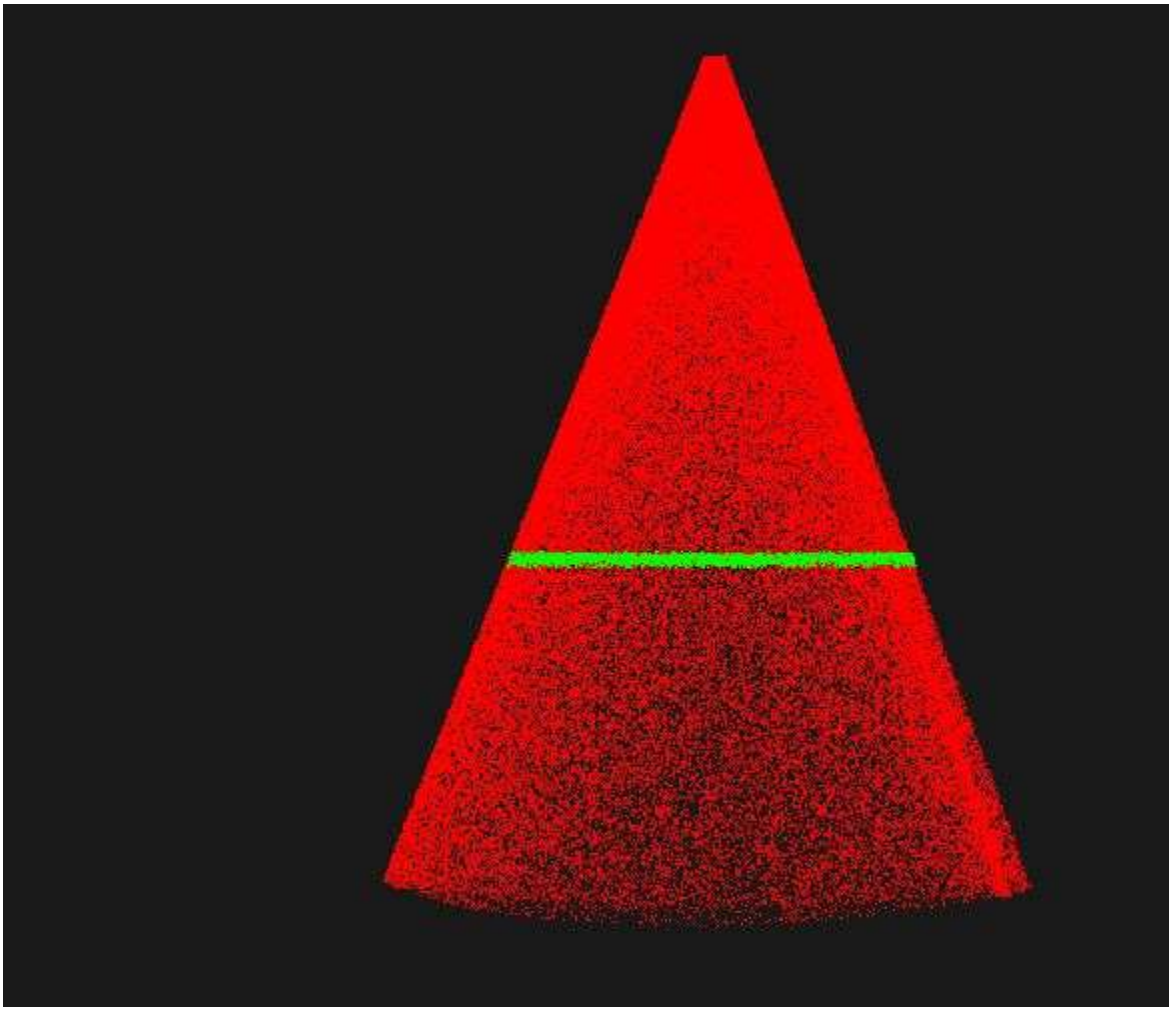

**Figure 2.5 Example of topographic-laser returns over Canso. The red points are erroneous noise and the green points are the water surface.**

The CH2 threw an error during the flight that required a partial system reboot. The error occurred within the sensor control unit (SCU) but did not affect trajectory collection or RCD30 operation. The reset caused the SCU settings to be reverted to their default. The 'peak threshold' setting controls amplitude of recorded energy required to qualify as a return. The default value for peak threshold (300) is much lower than our operational value (900) and this reversion caused the flood of noisy data. These setting also affected a portion of the Grand Manan collection (Figure 2.4). The additional data were cleaned using a specially developed algorithm and only minimally influenced the final survey results.

## 2.3 Ground Truth Data Collection

Ground truth data collection is an important aspect of topographic-bathymetric lidar data collection. In July 2016, AGRG researchers conducted traditional ground truth data collection in Canso and Big Basin including hard surface validation and depth measurements to validate the lidar, Secchi depth measurements for information on water clarity (Figure 2.8), and underwater photographs to obtain information on bottom type and vegetation. No ground truth data was collected on Deer Island (Figure 2.6). In Grand Manan, hard surface validation was collected using the RTK GPS system (Figure 2.9). Fieldwork for this project extended beyond the time of flight ground truth measurements.

The seabed elevation was measured directly using a large pole onto which the RTK GPS was threaded, in addition to manual measurements using a depth mate, a lead ball on a graduated rope, and a commercial-grade single beam echo sounder. By threading the RTK GPS antenna on the pole and measuring the elevation of the seabed directly we eliminated errors introduced into depth measurements obtained from a boat such as those caused by wave action, tidal variation, and angle of rope for lead ball drop measurements (Figure 2.7).
Table 2.2 summarizes the ground truth measurements undertaken for each of the study areas in 2016 and Figure 2.6 shows a map of the distribution of ground truth measurements.

A Seabird 25plus Conductivity Temperature Depth (CTD) sensor was used during the lidar survey on July 20 at Canso to measure changes in salinity, temperature, turbidity, and chlorophyll through the water column across each study area. The CTD data provided insight into the structure of the water column, such as whether it was well mixed or stratified which was valuable in evaluating lidar penetration. The data also provided an additional depth validation method (Figure 2.6).

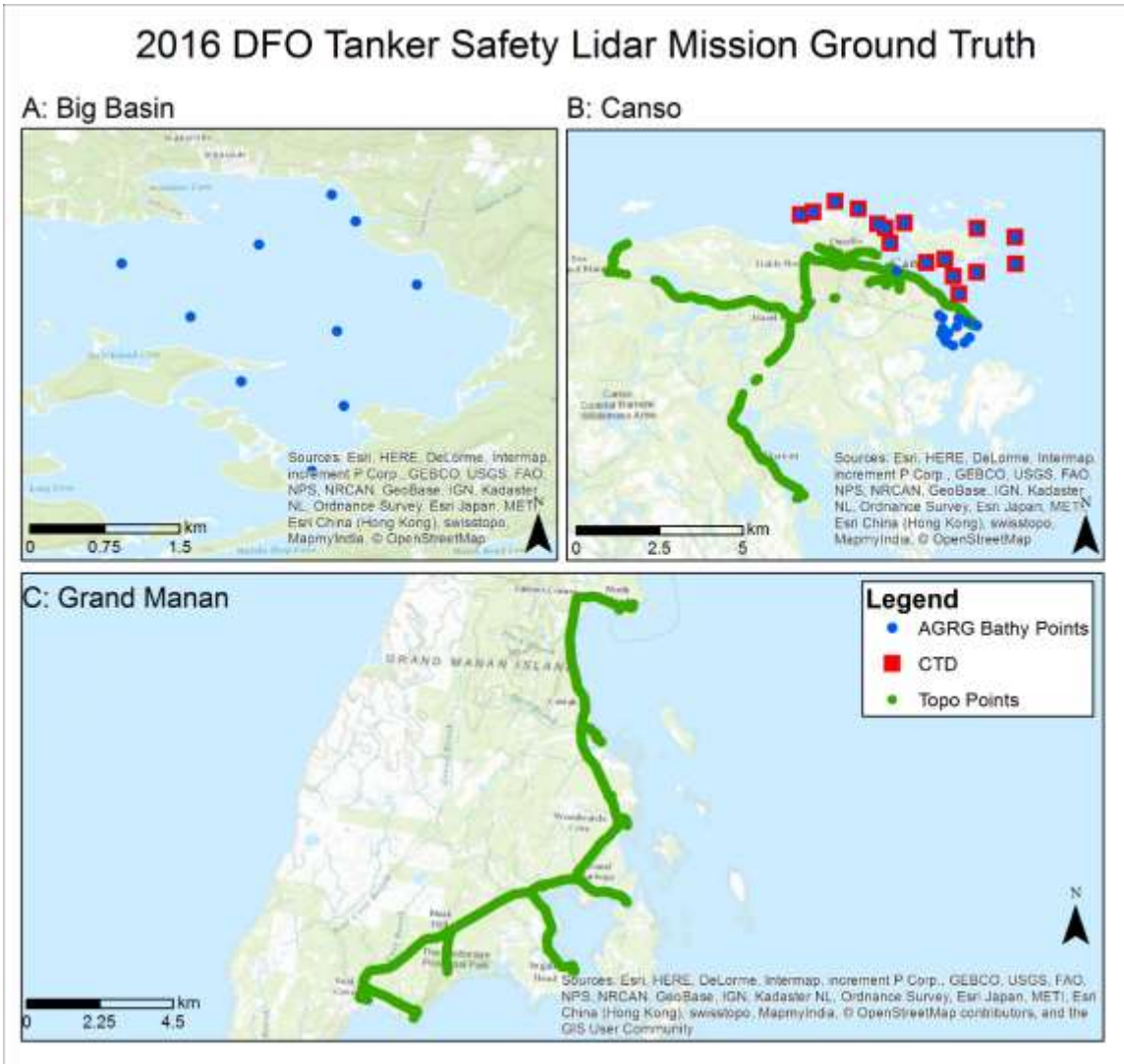


**Figure 2.6: Location of hard surface GPS validation points, AGRG boat-based ground truth points and CTD drops in the Tanker Safety study areas. Note that there was no ground truth collected in Deer Island.**

| Location | Date | Base Station (id) | GPS System | Secchi (Y or -) | Depth | Underwater Photos | Hard Surface GPS (Y or -) | CTD (Y or -) |
|---|---|---|---|---|---|---|---|---|
| **Big Basin** | Jul 14 | - | Garmin | Y | M, ES | $Q_{50}$ | - | - |
| **Canso** | Jul 20 | 210808 | GS14 | Y | P, M | $Q_{50}$ | Y | Y |
| **Deer Island** | - | - | - | - | - | - | - | - |
| **Grand Manan** | Aug 28 | 941020 | GS14 | - | - | - | Y | - |

**Table 2.2: Ground truth data summary. GPS Column: Two GPS systems were used, the Leica GS14 and a handheld Garmin unit. Depth Column: P=GPS antenna threaded onto the large pole for direct bottom elevation measurement; M=manual depth measurement using lead ball or weighted Secchi disk; ES=Single beam commercial grade Humminbird Echo Sounder; Underwater Photos: $Q_{50}$=0.25 $m^2$ quadrat with downward-looking GoPro camera.**

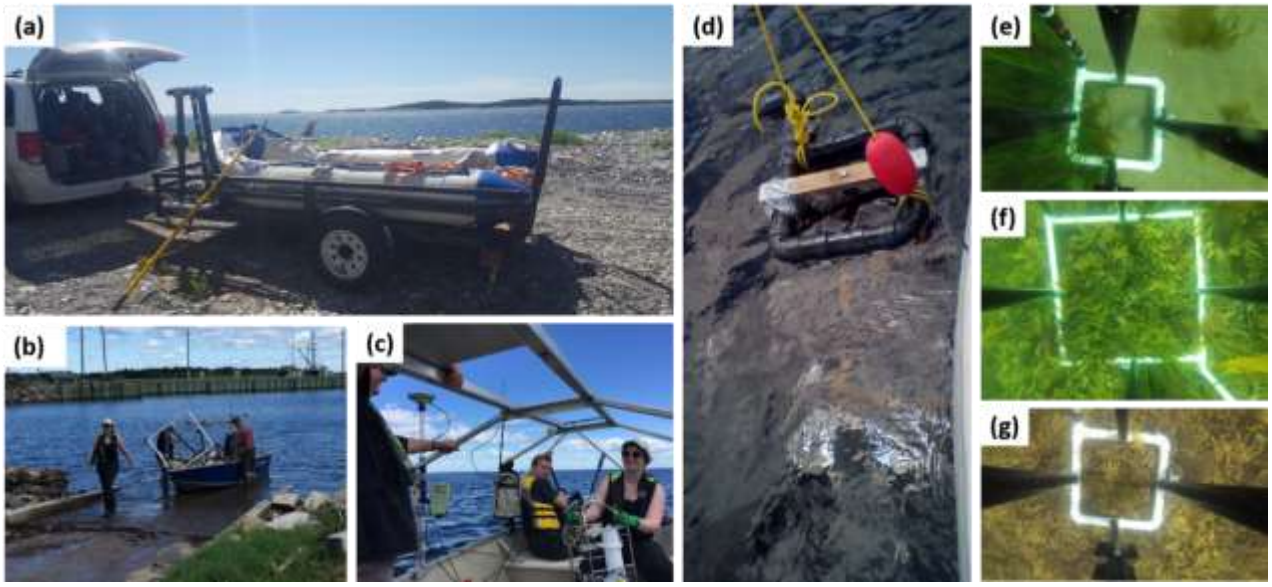


**Figure 2.7: Ground truth data collection at Canso (a), AGRG researchers conducting boat-based ground truth collection (b), CTD drops as part of ground truth collection (c), 0.25 $m^2$ quadrat collecting images of bottom type (d), ground truth survey results in Canso (e), (f) and (g).**

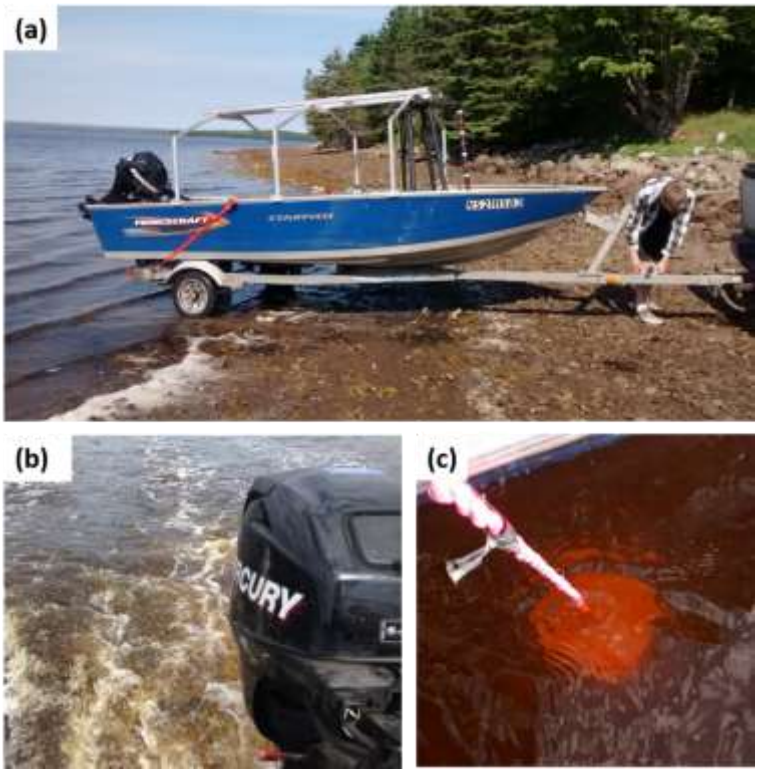


**Figure 2.8: Ground truth data collection at Big Basin (a), murky water during ground truth collection (b), limited Secchi clarity (c).**


**Figure 2.9: RTK GPS Hard surface validation at Grand Manan (a), lidar survey in Grand Manan at time of fieldwork (b), collecting validation on the beach (c), collecting validation in the parking lot (d), exposed vegetation at low tide (e).**

## 2.4 Time of Flight Conditions: Weather, Tide, and Turbidity

Meteorological conditions during and prior to topographic-bathymetric lidar data collection are an important factor in successful data collection. As the lidar sensor is limited by water clarity, windy weather has the potential to stir up any fine sediment in the water and prevent good laser penetration. Rainy weather is not suitable for lidar collection, and the glare of the sun must also be factored in for the collection of aerial photography. Before each lidar survey we primarily monitored weather forecasts using four tools: the Environment Canada (EC) public forecast (http://weather.gc.ca/) (Figure 1.1); EC's Marine Forecast (https://weather.gc.ca/marine/index_e.html ); SpotWx (www.spotwx.com), which allows the user to enter a precise location and choose from several forecasting models of varying model resolution and forecast length; and a customized EC forecast for the lidar study area provided to AGRG every eight hours. Each of these tools had benefits and shortcomings, and it was through monitoring all four that a successful lidar mission was achieved. For example, the customized EC forecast was the only tool that provided a fog prediction, on an hourly basis. However, the SpotWx graphical interface proved superior for wind monitoring. Only the EC public forecast alerted us to Weather Warnings that were broadcast in real-time, such as thunderstorms, and the marine forecast provided the only information for offshore conditions.

Big Basin was first surveyed on July 12 on a falling tide with winds blowing from the northwest at about 20 km/h throughout the survey. A second survey was completed for Big Basin on July 19 on a rising tide with winds blowing from the northwest at about 20 km/h, increasing to about 25 km/h throughout the survey (
Figure 2.10). Canso was surveyed on July 20 at high tide with winds blowing from the west at about 10 km/h, increasing to 20 km/h (
Figure 2.10). Deer Island was surveyed on July 6 at low tide with winds blowing from the north at about 10 km/h (Figure 2.11). Grand Manan, the largest island in the Bay of Fundy, required three individual surveys due to its size. The first survey was completed on August 28 at high tide, finishing at low tide. Winds were blowing from the south and increasing throughout the survey, from about 10 km/h to 30 km/h. The second survey was completed on September 17, beginning at low tide, and finishing on low tide. Winds were blowing from the south at about 20 km/h at the beginning of the survey, but increasing to about 35 km/h before decreasing again towards the end of the survey. The final Grand Manan survey was completed on September 26 at high tide, finishing at low tide. Winds were blowing from the north initially, at about 20 km/h, before shifting to the west, decreasing to about 10 km/h

(Figure 2.12).

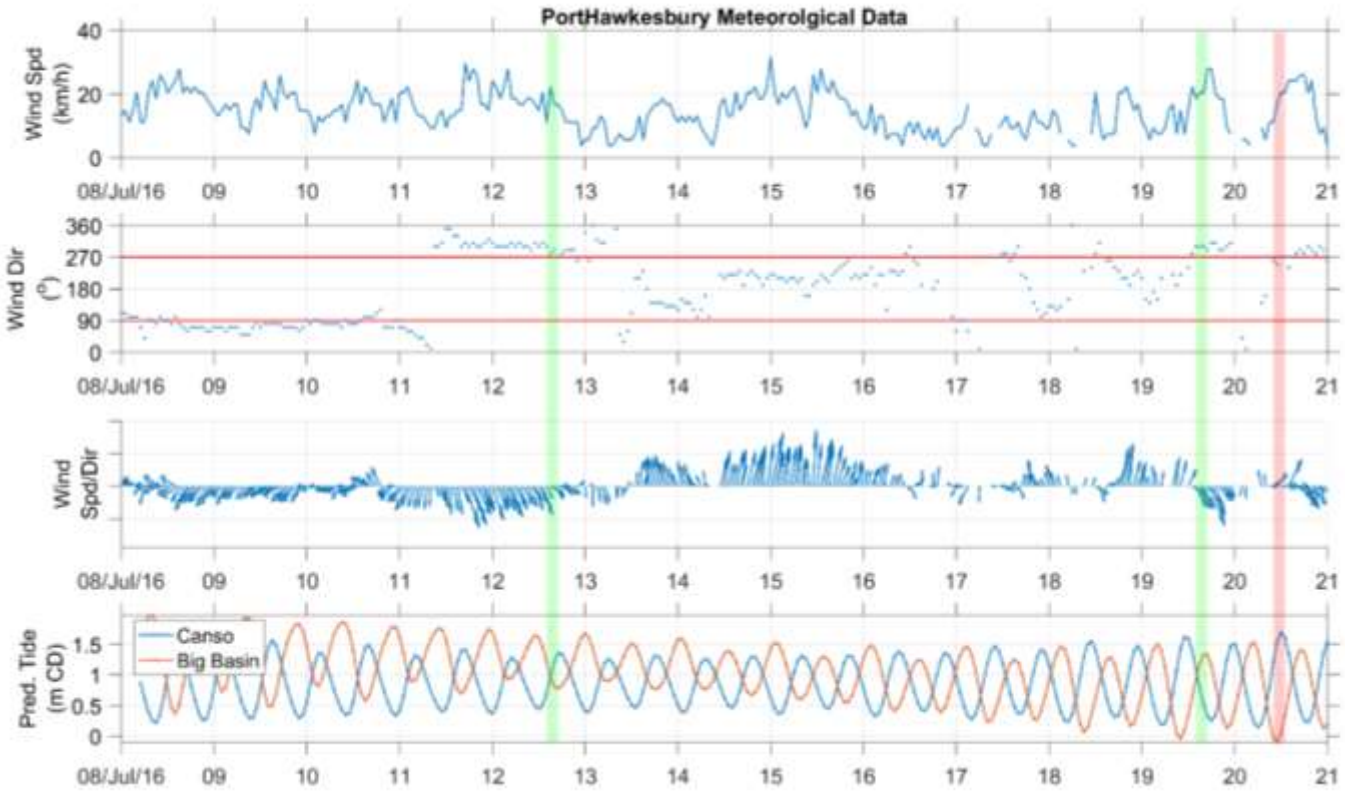


**Figure 2.10: (a) Wind speed and (b) direction collected at the EC weather station at Port Hawkesbury between July 8 and 21, 2016 at 1 hr intervals. Panel (c) shows a vector plot of the wind, where the arrows point in the direction the wind is blowing. Panel (d) shows the predicted tide at both Canso and Big Basin, symbolized accordingly. The red box indicates the lidar survey duration at Canso, and the green boxes at Big Basin.**

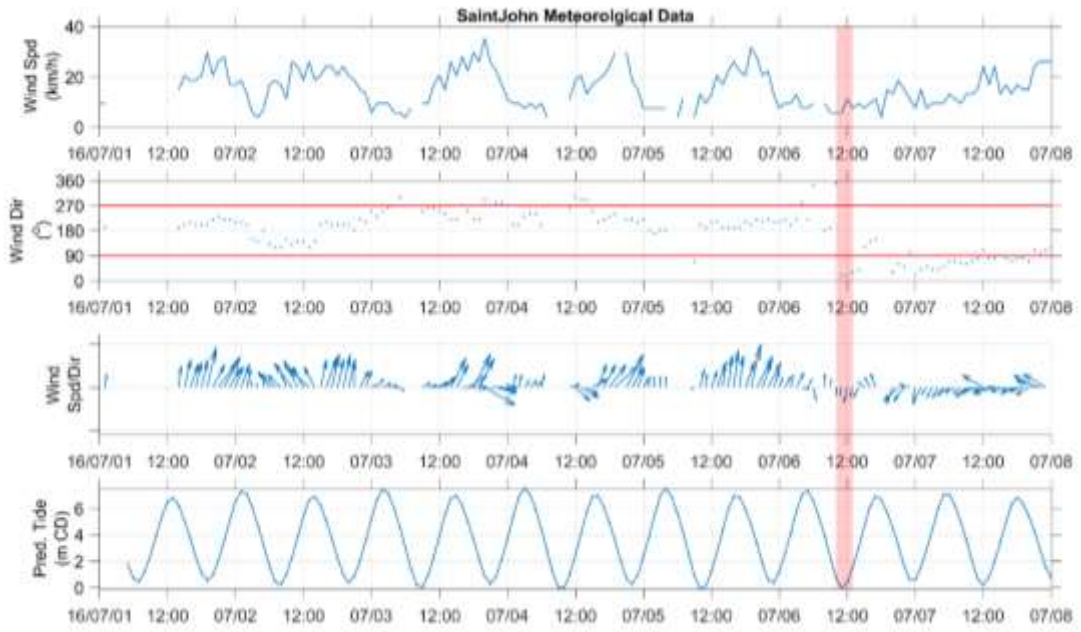


**Figure 2.11: (a) Wind speed and (b) direction collected at the EC weather station at Saint John between July 7 and 8, 2016 at 1 hr intervals. Panel (c) shows a vector plot of the wind, where the arrows point in the direction the wind is blowing. Panel (d) shows the predicted tide at Deer Island. The red box indicates the lidar survey duration at Deer Island.**

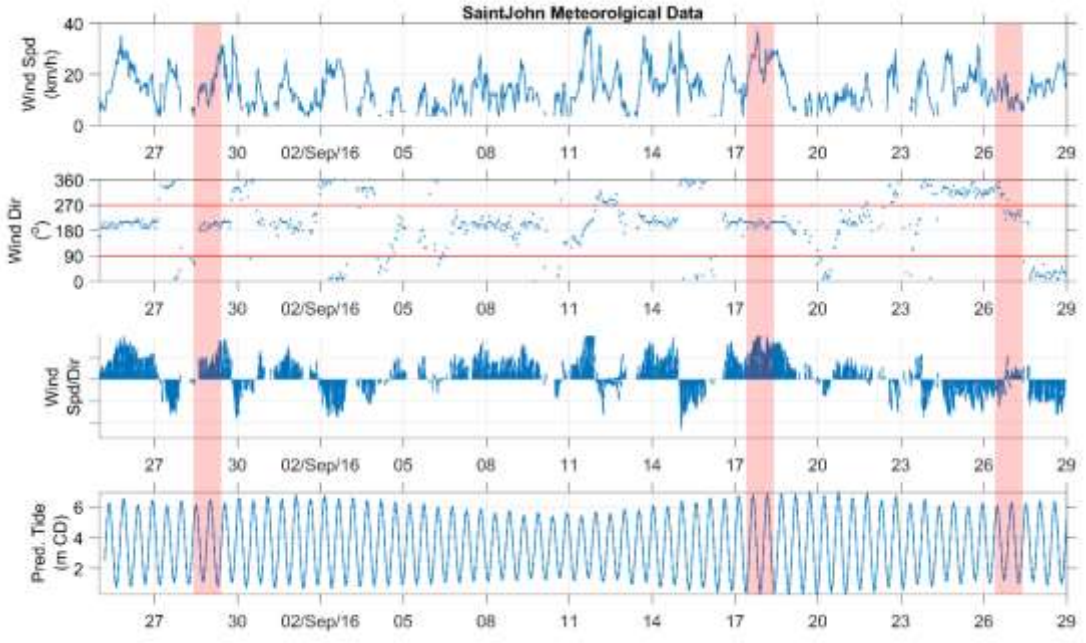


**Figure 2.12: (a) Wind speed and (b) direction collected at the EC weather station at Saint John between July 27 and 29, 2016 at 1 hr intervals. Panel (c) shows a vector plot of the wind, where the arrows point in the direction the wind is blowing. Panel (d) shows the predicted tide at Grand Manan. The red box indicates the lidar survey durations at Grand Manan.**

## 2.5 Elevation Data Processing

### 2.5.1 Lidar processing

#### *2.5.1.1 Point Cloud Processing*

Aircraft GPS data were differentially corrected using base station observations obtained from an active network or an established high precision monument in close proximity to the survey area. The aircraft trajectory was calculated by linking the corrected GPS data with the aircraft attitude measured by an inertial measurement unit (IMU). Lidar Survey Studio (LSS) was used to process Chiroptera II waveforms, which were georeferenced into discrete points by linking laser returns to the processed aircraft trajectory. The data were inspected to ensure there was sufficient overlap (30%) and no gaps exist in the lidar coverage.

One critical step in the processing of bathymetric lidar is the ability to map the water surface. This is critical for two components of georeferencing the final target or targets that the reflected laser pulse recorded: the refraction of the light when it passes from the medium of air to water and the change in the speed of light from air to water. The LSS software computes the water surface from the lidar returns of both the topo and bathy lasers. In addition to classifying points as land, water surface, or bathymetry; the system also computes a water surface that ensures the entire area of water surface is covered regardless of the original lidar point density. As mentioned, part of the processing involves converting the raw waveform lidar return time series into discrete classified points using LSS signal processing; points include ground, water surface, seabed, etc. Waveform processing may include algorithms specifically for classifying the seabed. The points were examined in LSS both in plan view and in cross-section view. The waveforms can be queried for each point so that the location of the waveform peak can be identified and the type of point defined, for example water surface and bathymetry.

The LAS files were read into TerraScan™ with the laser returns grouped by laser type so they could be easily separated, analyzed, and further refined. Because of the differences in the lidar footprint between the topo and bathy lasers, the bathy point returns would be used to represent the water surface and bathymetry points and the topo points would be used to represent targets on the land. See Table 2.3 and the attached Data Dictionary report for the classification codes for the delivered LAS 1.2 files. The refined classified LAS files were read into ArcGIS™ and a variety of raster surfaces at a 1 m spatial sampling interval were produced.

| Class number | Description |
|---|---|
| 0 | Water model |
| 1 | Bathymetry (Bathy) |
| 2 | Bathy Vegetation |
| 3 | N/A |
| 4 | Topographic (Topo) laser Ground |
| 5 | Topo laser non-ground (vegetation & buildings) |
| 6 | Hydro laser Ground |
| 7 | Bathy laser non-ground |
| 8 | Water |
| 9 | Noise |
| 10 | Overlap Water Model |
| 11 | Overlap Bathy |
| 12 | Overlap Bathy Veg |
| 13 | N/A |
| 14 | Overlap Topo Laser Ground |
| 15 | Overlap Topo Laser Veg |
| 16 | Overlap Bathy Laser Ground |
| 17 | Overlap Bathy Laser Veg |
| 18 | Overlap Water |
| 19 | Overlap Noise |

**Table 2.3: Lidar point classification Codes and descriptions. Note that 'overlap' is determined for points which are within a desired footprint of points from a separate flight line; the latter of which having less absolute range to the laser sensor.**

#### *2.5.1.2 Gridded Surface Models*

There are three main data products derived from the lidar point cloud. The first two are based on the elevation and include the Digital Surface Model (DSM), which incorporates valid lidar returns from vegetation, buildings, ground, and bathymetry returns; and the Digital Elevation Model (DEM), which incorporates ground returns above and below the water line. The third data product is the intensity of the lidar returns, or the reflectance of the bathymetric laser. The lidar reflectance, or the amplitude of the returning signal from the bathymetric laser, is influenced by several factors including water depth, the local angle of incidence with the target, the natural reflectivity of the target material, the transmission power of the laser, and the sensitivity of the receiver.

#### *2.5.1.3 Depth Normalization of the Green Laser*

The amplitude of the returning signal from the bathymetric laser provides a means of visualizing the seabed cover, and is influenced by several factors including water depth and clarity, the local angle of incidence with the target, the natural reflectivity of the target material, and the voltage or gain of the transmitted lidar pulse. The raw amplitude data are difficult to interpret because of variances as a result of signal loss due to the attenuation of the laser pulse through the water column at different scan angles. Gridding the amplitude value from the bathymetric laser results in an image with a wide range of values that are not compensated for depth and have significant differences for the same target depending on the local angle of incidence from flight line to flight line. As a result, these data are not usable as is for quantitative analysis and are difficult to interpret for qualitative analysis. A process has been developed to normalize the amplitude data for signal loss in a recent publication (Webster et al., 2016). The process involved sampling the amplitude data from a location with homogeneous seabed cover (e.g., sand or eelgrass) over a range of depths. These data were used to establish a relationship between depth and the logarithm of the amplitude value. The inverse of this relationship was used with the depth map to adjust the amplitude data so that they could be interpreted without the bias of depth. A depth normalized amplitude/intensity image (DNI) was created for the study site using this technique that can be more consistently interpreted for the seabed cover material. Note that this analysis considers only bathymetric lidar values and ignores any topographic elevation points.

#### *2.5.1.4 Aerial Photo Processing*

The RCD30 60 MPIX imagery was processed using the aircraft trajectory and direct georeferencing methodology within the PhotoScan Professional software package by Agisoft. Direct georeferencing requires a known camera orientation at the time of the photo and a source of correction for displacement of light caused by relief and lens distortion. Lidar data were processed to produce bare-earth digital elevation models that were used to remove displacement caused by relief in the orthorectification process. Photo orientations were calculated by linking the exterior orientation (EO) extracted from the aircraft trajectory GPS position (X, Y, Z) and the IMU attitude (omega, phi, kappa) at shutter event to the engineered internal orientation (IO) of the RCD30 (CCD dimensions, focal length, lens curvature).

### 2.5.2 Ellipsoidal to Orthometric Height Conversion

The original elevation of any lidar products are referenced to the same elevation model as the GPS they were collected with. This model is a theoretical Earth surface known as the ellipsoid, and elevations referenced to this surface are in ellipsoidal height (GRS80). To convert them to orthometric height (OHt), which is height relative to the Canadian Geodetic Vertical Datum of 1928 (CGVD28), an offset must be applied. The conversions are calculated based on the geoid-ellipsoid separation model, HT2, from Natural Resources Canada.

## 2.6 Lidar Validation

Ground elevation measurements obtained using the RTK GPS system were used to validate the topographic lidar returns on areas of hard, flat surfaces. In Canso and Grand Manan, the GPS antenna was mounted on a vehicle and data were collected along roads within the study areas, and points were collected manually along wharves in Grand Manan (green lines on Figure 2.6).

Boat-based ground truth data were used to validate the bathymetric lidar returns in Canso and Big Basin (blue dots on Figure 2.6). Although various methods were used to measure depth during fieldwork, ( Table 2.2), for this report only points measured using the large pole fitted with the RTK GPS antenna to directly measure the seabed elevation were used for the accuracy assessment; points that measured depth using sonar or a weighted rope were not considered at this time.

For both hard surface and boat-based GPS points, the differences in the GPS elevation and the lidar elevation (ΔZ) were calculated by extracting the lidar elevation from the DEM at the checkpoint and subtracting the lidar elevation from the GPS elevation. GPS points were subject to a quality control assessment such that the standard deviation of the elevation was required to be < 0.05 m.

## 2.7 Bottom Type Classification

The full cover types and the submerged aquatic vegetation (SAV) maps were derived from the lidar and QA orthophotos. The layers used included the water depth, derived from the DEM and water surface at the time of flight; depth normalized intensity; and arithmetic combinations of the true-color QA camera orthophoto mosaic. As mentioned, the 20 cm QA photos provide a more consistent level of detail in the water than the RCD30 photos, so the QA photos were used in the seabed mapping (Figure 2.13). Ratios of the different RGB band differences and their sums were utilized in similar fashion as a traditional Normalized Difference Vegetation Index (NDVI) using red and NIR imagery. The bottom cover map represents an index of vegetation presence that is then further interpreted for bottom vegetation type

and substrate type. This complex map was then simplified to produce a simpler Submerged Aquatic Vegetation (SAV) as well. This method was used to classify the material that were submerged during the survey.

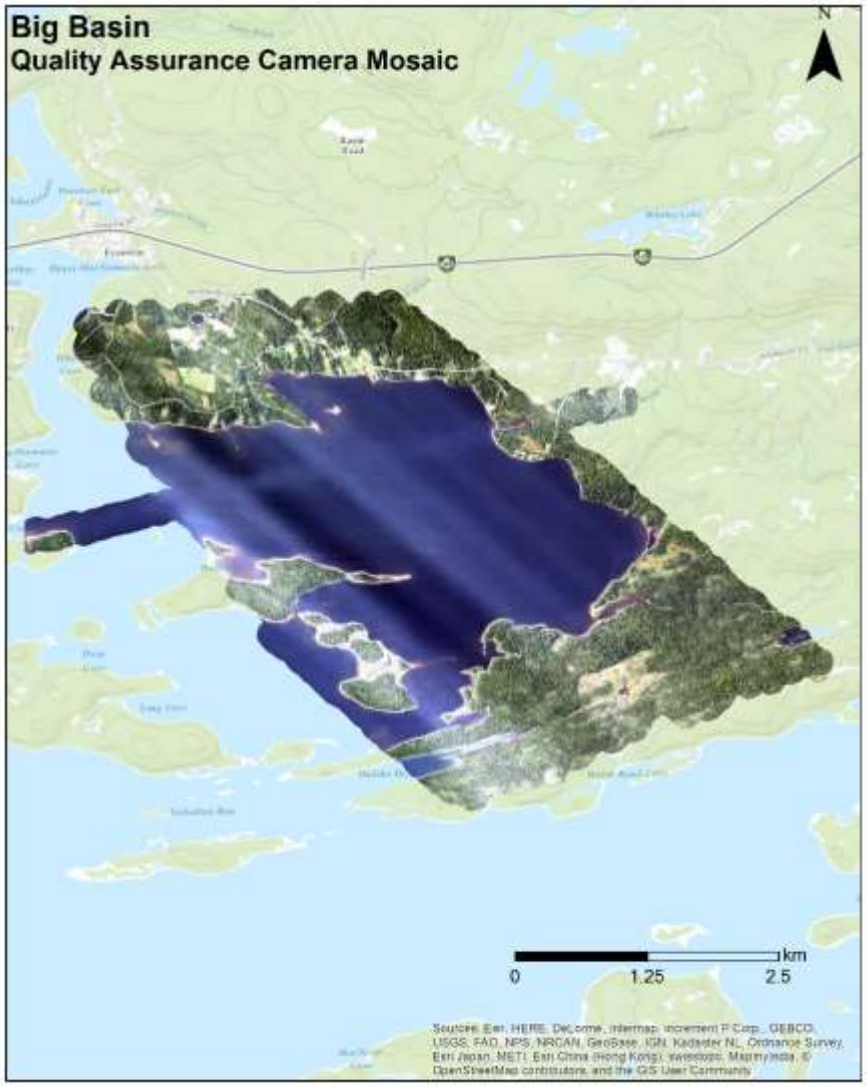


**Figure 2.13: Example of the 20cm QA orthophoto mosaic used in the bottom classification.**

Another classification method focused on the exposed shoreline material that may be vulnerable to contamination in the event of a spill. Here, texture and spectral details of the RCD30 imagery were used to classify the beach materials, which included true colour (Figure 2.14), and NIR false colour (Figure 2.15) and the details are discussed below.


**Figure 2.14: Example of the RCD30 orthophoto mosaic in true colour RGB.**

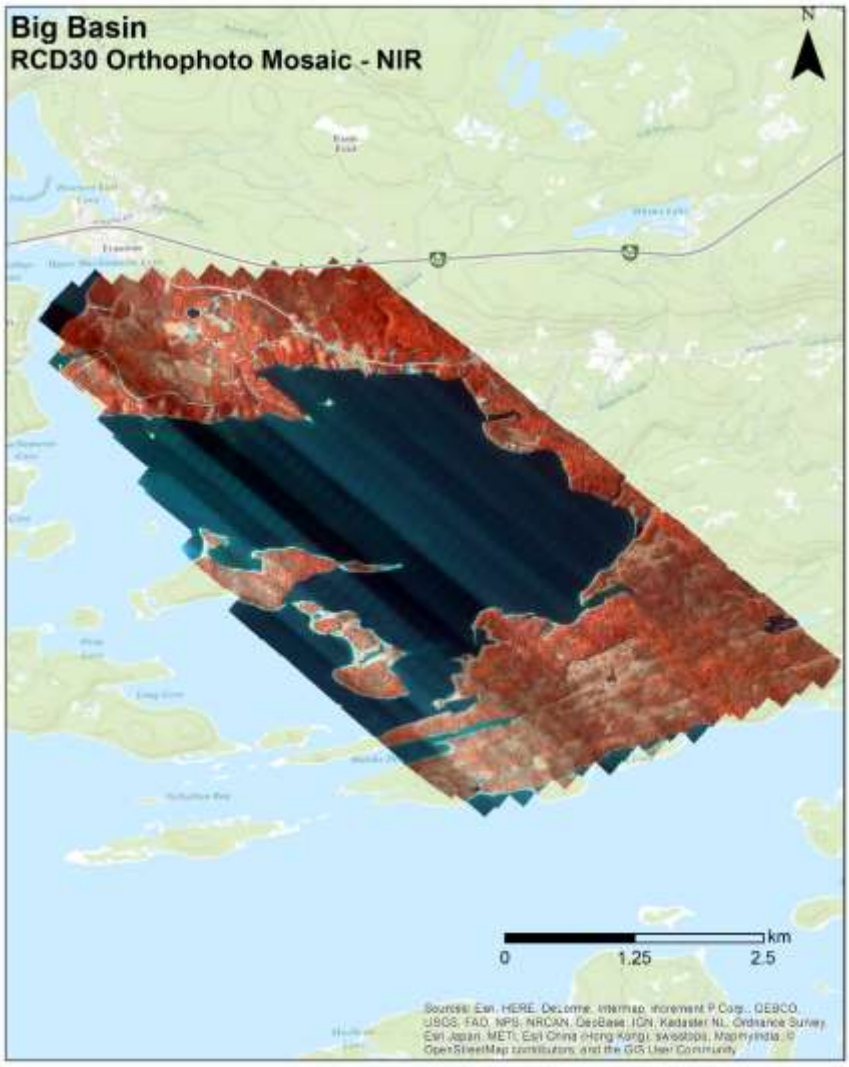


**Figure 2.15: Example of the RCD30 orthophoto mosaic in false colour NIR to highlight the exposed vegetation.**

## 2.8 Shoreline Classification

Shoreline substrates, such as cobble and sand, are defined by their grain sizes rather than their chemical compositions. This is due to the fact that they are typically derived from the same parent materials. As such, their spectral characteristics are quite similar and cannot be used as the sole basis for a robust classification. In order to achieve the latter, it is necessary to take image texture into account as well. In this analysis, image texture was quantified by means of a line density filter. In natural imagery, lines appear at the boundaries of objects (ex. boulders) and as such are analogous to edges. Theoretically, larger and brighter materials (ex. cobble) will produce stronger edges than finer ones (ex. sand), allowing them to be differentiated. This edge density raster was produced in the following way. Firstly, a series of

line detectors were convolved over the image, detecting all lines oriented at 0, 45, 90, and 125 degree angles in the RCD30 imagery. This produced 4 different rasters per image frame, each representing the intensity of the edges in the image that shared that specific orientation. These four rasters were averaged on a cell-by-cell basis and smoothed using a 9x9 mean filter to produce the final edge density raster. Iterating the line detector over different angles was necessary in order to ensure that the edge density metric was rotation-invariant, and as such sufficiently robust for use in the subsequent classification.

A Normalized Difference Vegetation Index (NDVI) layer was also derived from the RCD30 imagery and included in the classification, which is calculated from the NIR and red bands. Firstly, it was used as a mask to narrow down the spatial extent of the region to be classified. Any image region with an NDVI above 0.40 was assumed to be vegetation and was therefore removed from further analysis. This greatly reduced the amount of data that needed to be processed, speeding up the analysis significantly. Once the image had been classified statistically, these high NDVI regions were defined as vegetation and appended to the classified image.

The NDVI was also included in the classification. The rationale for this was as follows. Firstly, rocky materials have low NDVIs whereas vegetation tends to have very high NDVI values. As such, NDVI provides a concise descriptor of the amount of rocky material that is exposed in regions with vegetation cover (ex. swash zone). Rocky materials with vegetation on them tend to appear darker, and as such have weaker edges than they would without it. As such, based on the texture alone cobble with vegetation on it could statistically be closer to dry pebbles than it would be to dry cobble. Adding the NDVI takes this phenomenon into account, increasing the reliability of the classified results.

The NDVI and edge density rasters were then used in conjunction with multispectral RCD30 imagery bands in the context of a supervised Maximum Likelihood classification (
Figure 2.16). In order to account for illumination changes over the course of the aerial survey, this classification was done on a per-flightline basis. This assumes that light and water conditions were unlikely to change significantly over the period of time needed to fly a single flightline. As such, the frames collected during a flightline are more similar in those respects to one another than they are to the frames of other flightlines. This greatly reduced the number of artifacts in the final classification, particularly if the imagery was acquired in variably cloudy conditions. One of the limitations of this approach was that it was difficult to reliably differentiate bedrock from similar classes. For example, very smooth bedrock was commonly confused for sand whereas rough bedrock was often mistaken for

boulders. As such, the bedrock class was removed from the classification and outcrops of that nature were digitized manually.

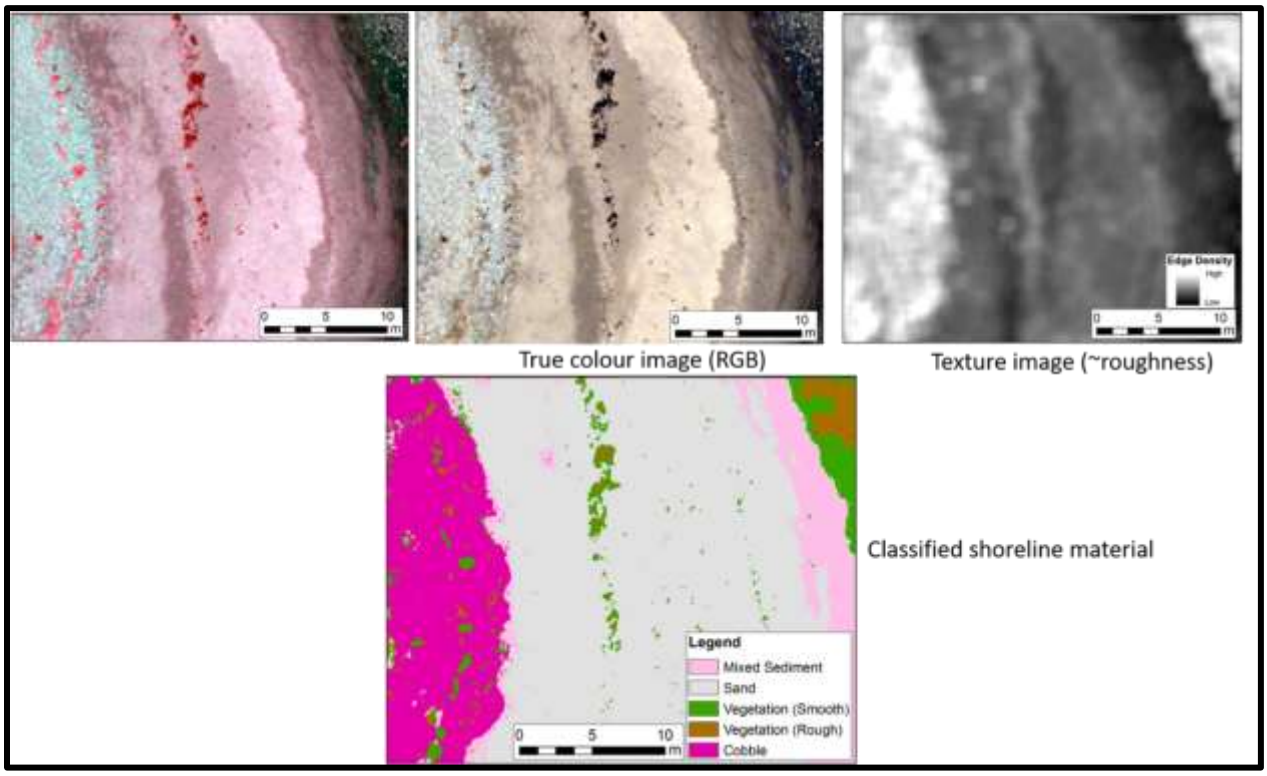


**Figure 2.16: Example of input bands for shoreline classification. (Note: the NDVI is not included in the figure).**

## 2.9 Submerged Aquatic Vegetation Maps

The SAV map was derived from the lidar and orthophotos and included the water depth raster, derived from the DEM; lidar bottom reflectance intensity; and the true-color aerial photograph orthomosaic. The approach used the red and green imagery bands, which were extracted from the true-color aerial photograph orthomosaic. Ratios of their differences and of their sums were added together and weighted by the interlaced lidar intensity data. The result was then normalized by the effects of depth. The resulting raster represents vegetation presence index and was subject to a threshold procedure to result in a final shapefile of vegetation presence or absence (Figure 2.17). The procedure to produce the final SAV map involved manually editing the shapefile using the RGB photos for interpretation, and included removing shadows created by overlapping trees in the imagery and clipping of the dataset to the relevant area.

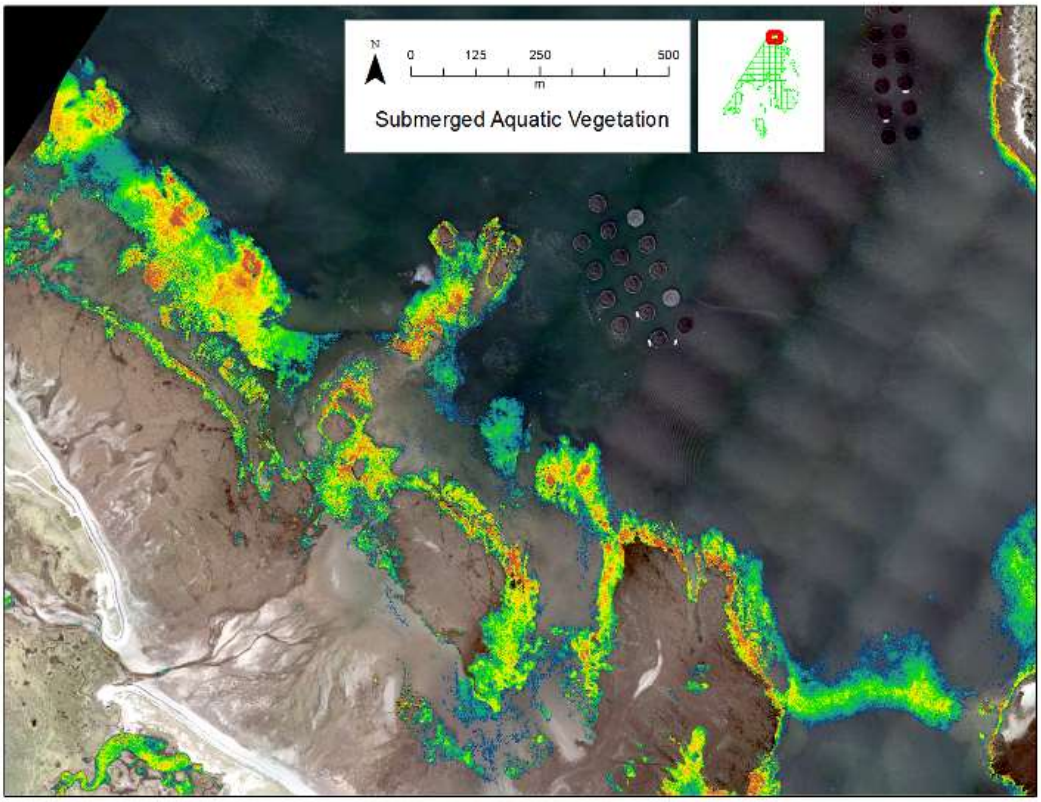


**Figure 2.17: Submerged Aquatic Vegetation (SAV) mapped near aquaculture in Grand Manan.**

## 2.10 Hydrodynamic Model

A high-resolution 2-D hydrodynamic (HD) model is under development that will incorporate lidar data within the Canso and Isle Madame areas. The DHI Mike-21™ modelling package will simulate current flow and water level variations within the Chedabucto Bay study area. The Mike software includes the capability to simulate the transport and fate of dissolved and suspended substances discharged or accidentally spilled within the region. The model domain will be much larger than the two lidar study areas to ensure there is sufficient surrounding bathymetry to properly simulate water circulation around these high-resolution areas. The domain will incorporate the region from the mouth of Chedabucto Bay into the complex shoreline near Isle Madame and up the Strait of Canso as far as the Canso Causeway.

A variety of topographic and bathymetric data sources compiled at variable resolutions were used to develop the model surface. The finest resolution dataset was the lidar data surveyed by AGRG in 2014/2015/2016 resampled to 3 m resolution for computational efficiency. Other bathymetry data included a digital compilation of bathymetry data from various sources (multibeam and single beam echo sounders) aggregated by CHS (Varma et al., 2008) at between 5 and 20 m resolution; paper chart 4335

(scale 1:75,000) was purchased and digitized manually and chart 4307 (scale 1:37,500) was purchased as an Electronic Navigational Chart (ENC). Topography not included in the lidar dataset were complied at 30 m resolution from shuttle radar topography mission (SRTM) data. The bathymetric and topographic datasets were merged separately using an interpolation method developed at AGRG. The algorithm ensured that very low-resolution data (800 m) are up-sampled to higher resolution (3 m) while minimizing the interpolation artifacts in the areas where data do not exist.

The nested grid approach reduced the complexity and number simulation calculations resulting in a more efficient and stable model. This technique effectively reduced the resolution of model input data in regions distant from the main areas of interest (AOI) by nesting high-resolution AOI grids within low resolution 'background' grids at 3:1 resolution steps (Figure 2.18, Figure 2.19).

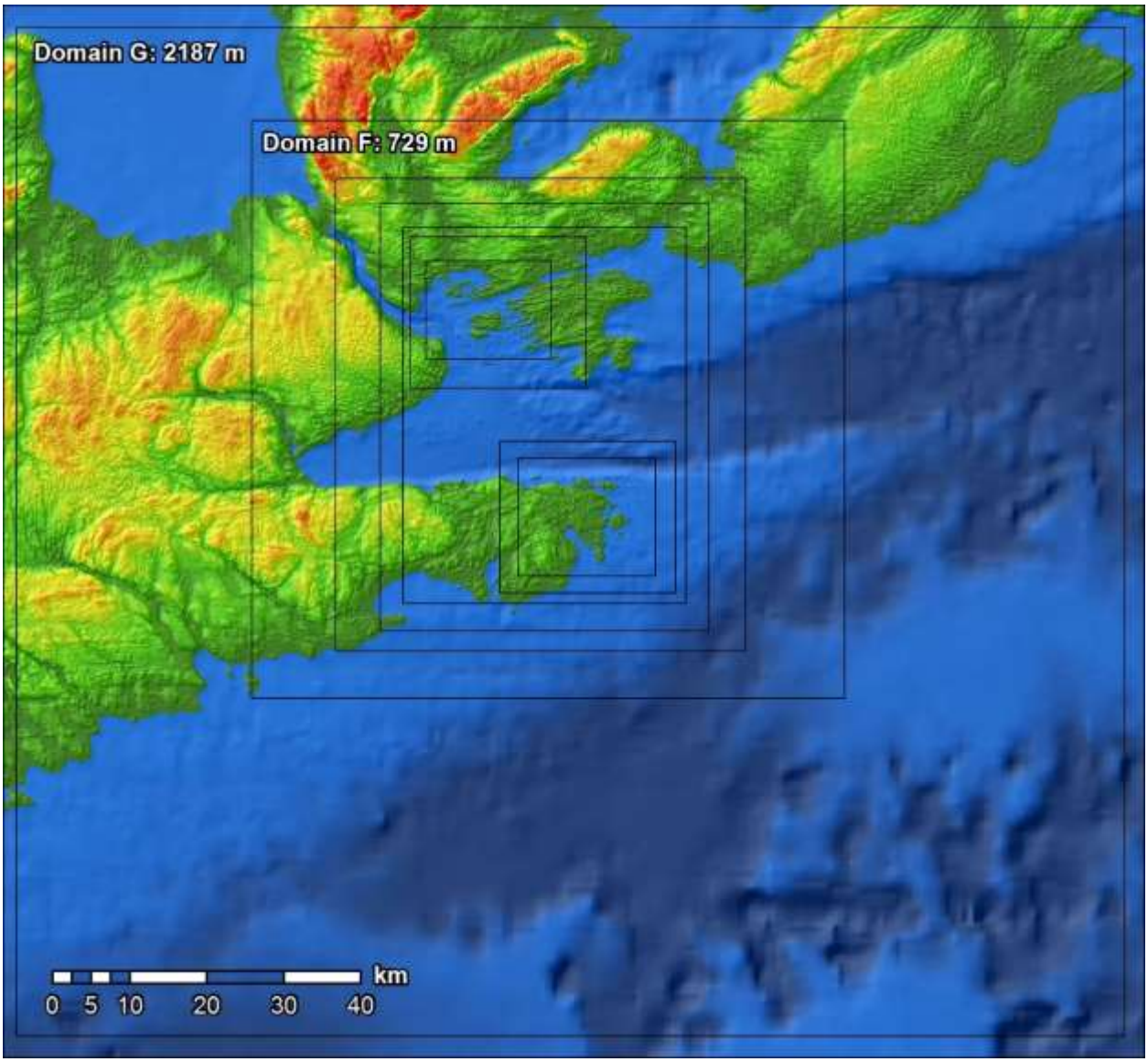


**Figure 2.18: Nested model domain to support Mike 21 simulations.**

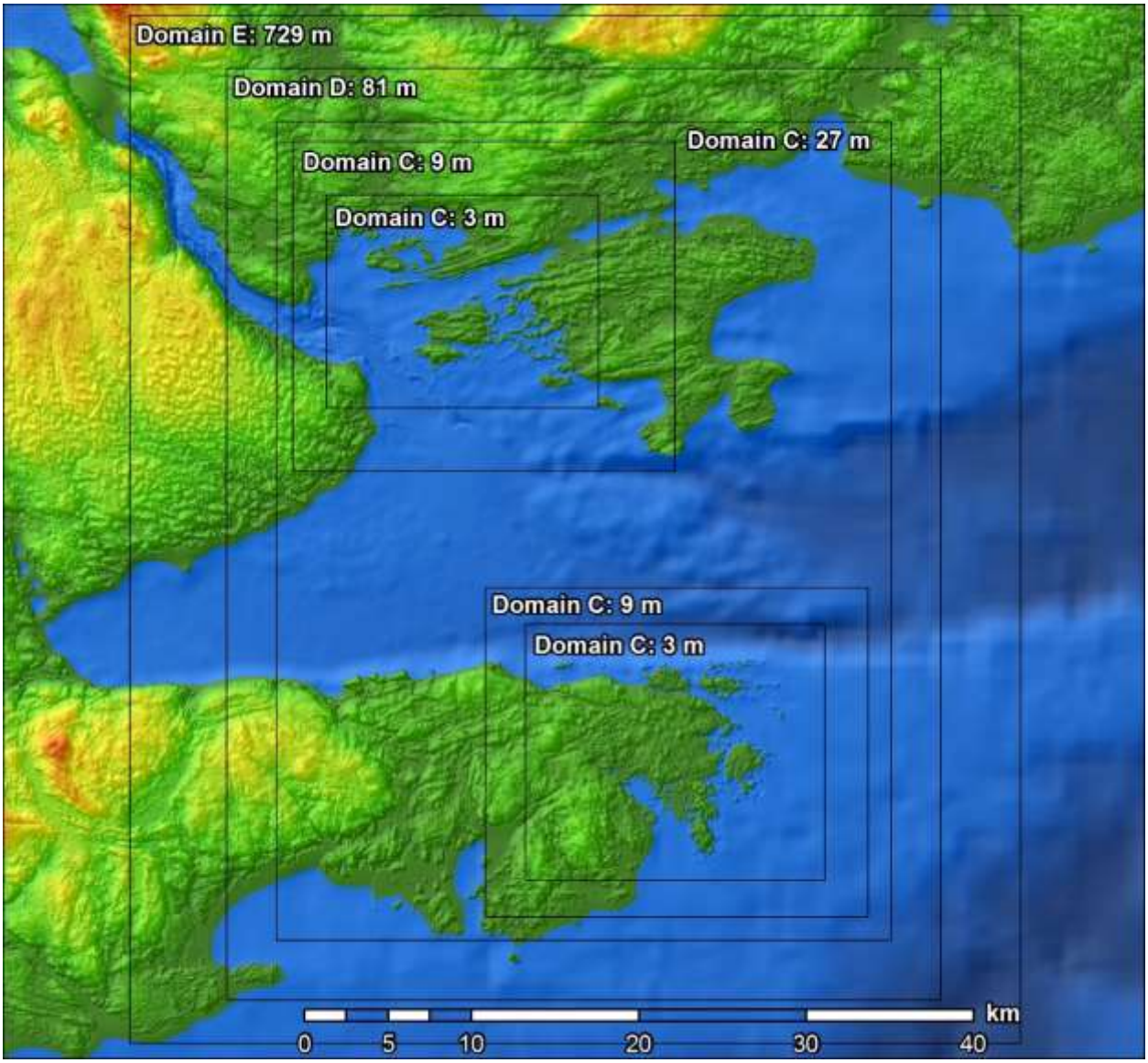


**Figure 2.19: Chedabucto Bay model domain.**

The model simulated water level variations over interpolated bathymetry in response to tidal forcing at the model boundaries. Predictions of tidal state were calculated at 5-minute temporal resolution using the WebTide software package (Dupont *et al.*, 2005). The nested grid approach ensured that the model domain was large enough that tidal boundaries were distant to the AOIs and reduced the inaccuracies inherent in these predictions.

# 3 Results

## 3.1 Lidar Validation

### 3.1.1 Topographic Validation

In Grand Manan, there were 1216 points collected along the roads and wharves within the study area with a calculated mean ΔZ of -0.11 m ± 0.02 m.

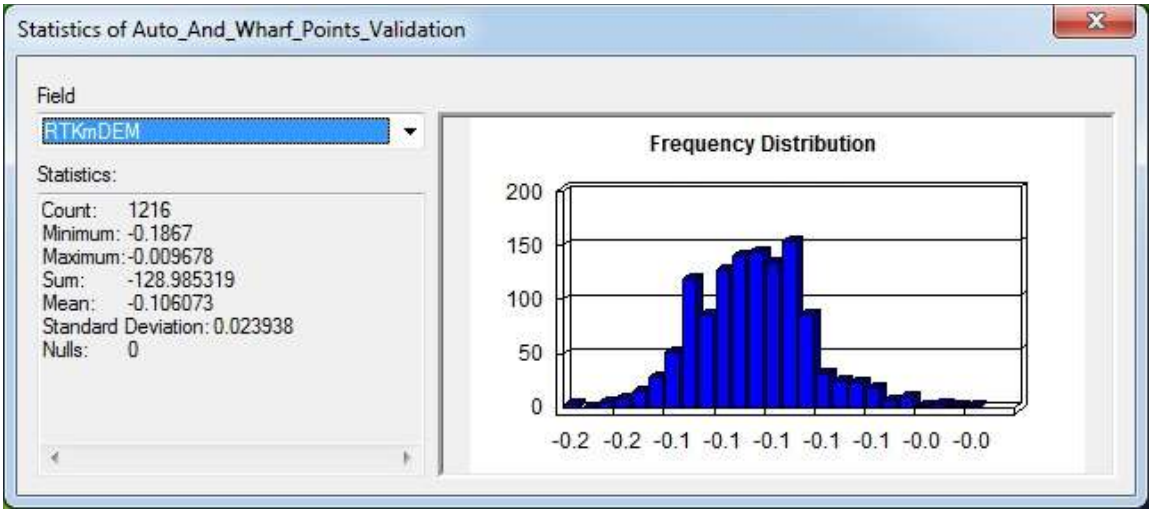


**Figure 3.1: Topographic lidar validation for Grand Manan.**

In Canso, there were 3718 points collected along the roads within the study area with a calculated mean ΔZ of -0.04 m ± 0.04 m.

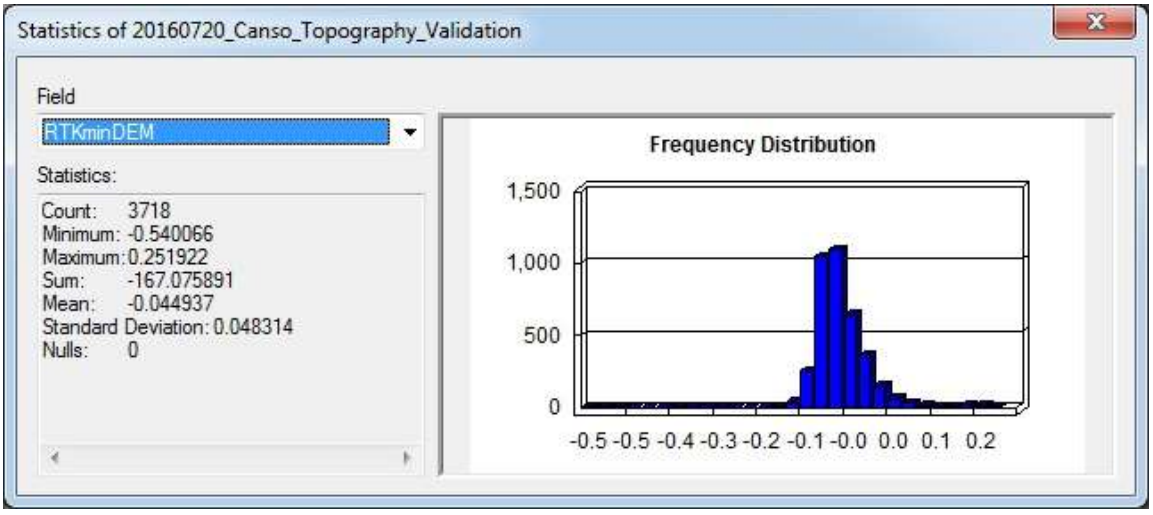


**Figure 3.2: Topographic lidar validation for Canso.**

### 3.1.2 Bathymetric Validation

In Canso, there were 11 points collected within the study area with a calculated mean ΔZ of -0.09 m ± 0.21 m.

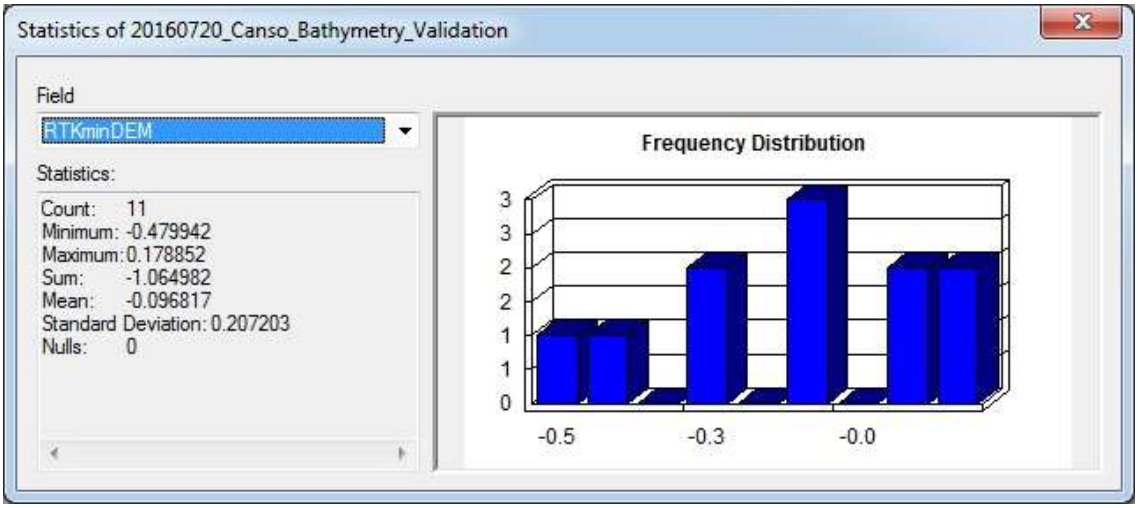


**Figure 3.3: Bathymetric lidar validation for Canso.**

## 3.2 Surface Models and Air Photos

The following section will present the results of surface models and air photos for each of the study areas derived from the lidar surveys.

### 3.2.1 Big Basin

The lidar survey at Big Basin penetrated to a minimum elevation of -4.94 m CGVD28 in the southern portion of the study area (Figure 3.4). The lidar did not penetrate to the bottom in the center of the Basin. This is likely due to a combination of deep bathymetry, vegetation, and murky water caused by high winds leading up to the survey. The Digital Elevation Model (DEM) shows the topography relief in shades of green-yellow-red and the bathymetry relief in light blue. The Colour Shaded Relief (CSR) model shows the topography and bathymetry relief in the same colours as the DEM but provides an exaggerated relief model (5 times actual height) and artificial shading to accentuate topographic and bathymetric features (Figure 3.5) provided in the DEM. The shades of darker blue represent deeper water.

The orthophoto mosaic provides insight into land use, water clarity, bottom type, wave action, and river morphology (Figure 3.6). The dark water in the center of the Basin confirms that the water was likely too deep and/or murky for the lidar to penetrate during the survey. The panels provide a closer look at the water clarity in the study area.

The Depth Normalized Intensity model (DNI) can be a powerful tool to reveal submerged features and bottom type information that are challenging for the air photos to depict. The intensity data show the contrast between brightly coloured seabed and the dark colour of submerged vegetation. Figure 3.7 shows the 1m intensity before depth normalizing, while Figure 3.8 shows the depth normalized intensity. Submerged features become much clearer after depth normalization, and it is possible to see more detail in the nearshore areas as pictured in the inset areas.

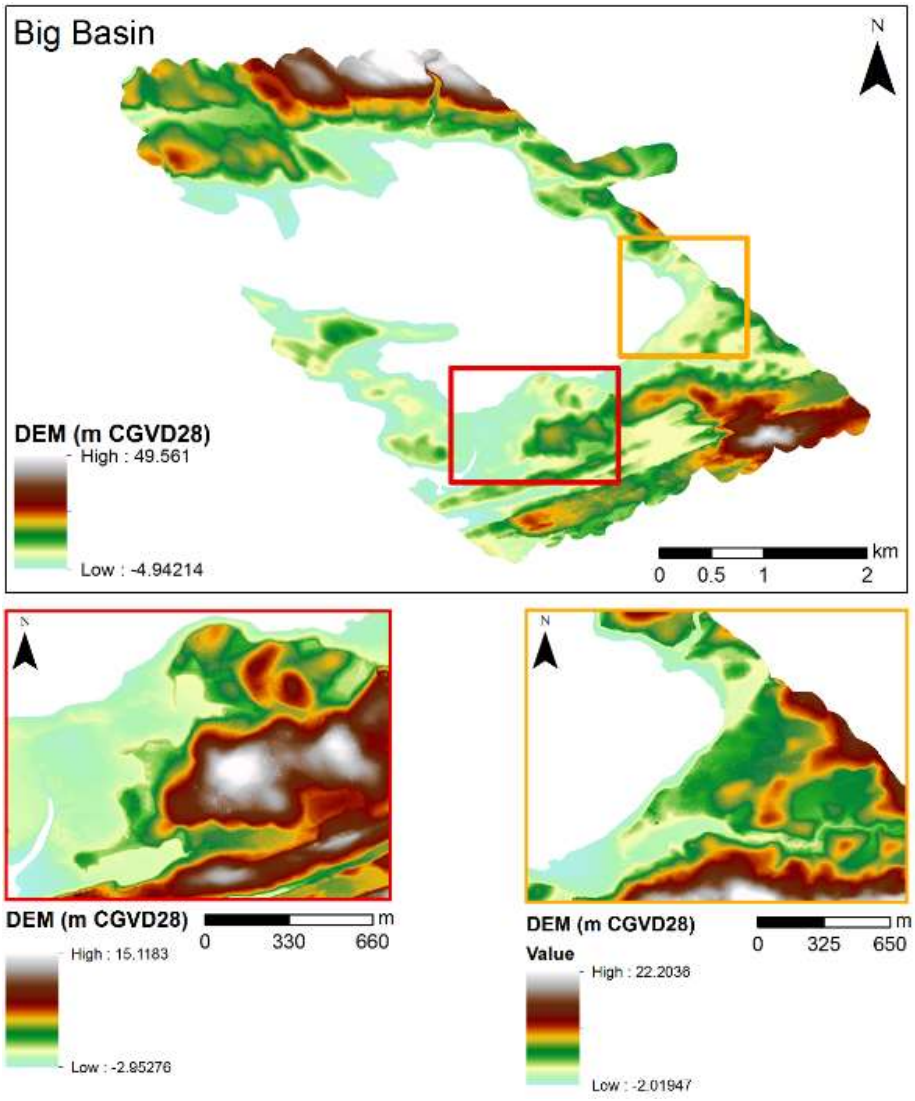


**Figure 3.4: Big Basin Digital Elevation Model, scaled to show bathymetry relief, and with insets showing smaller features. Insets are matched to the larger figure by border colour.**

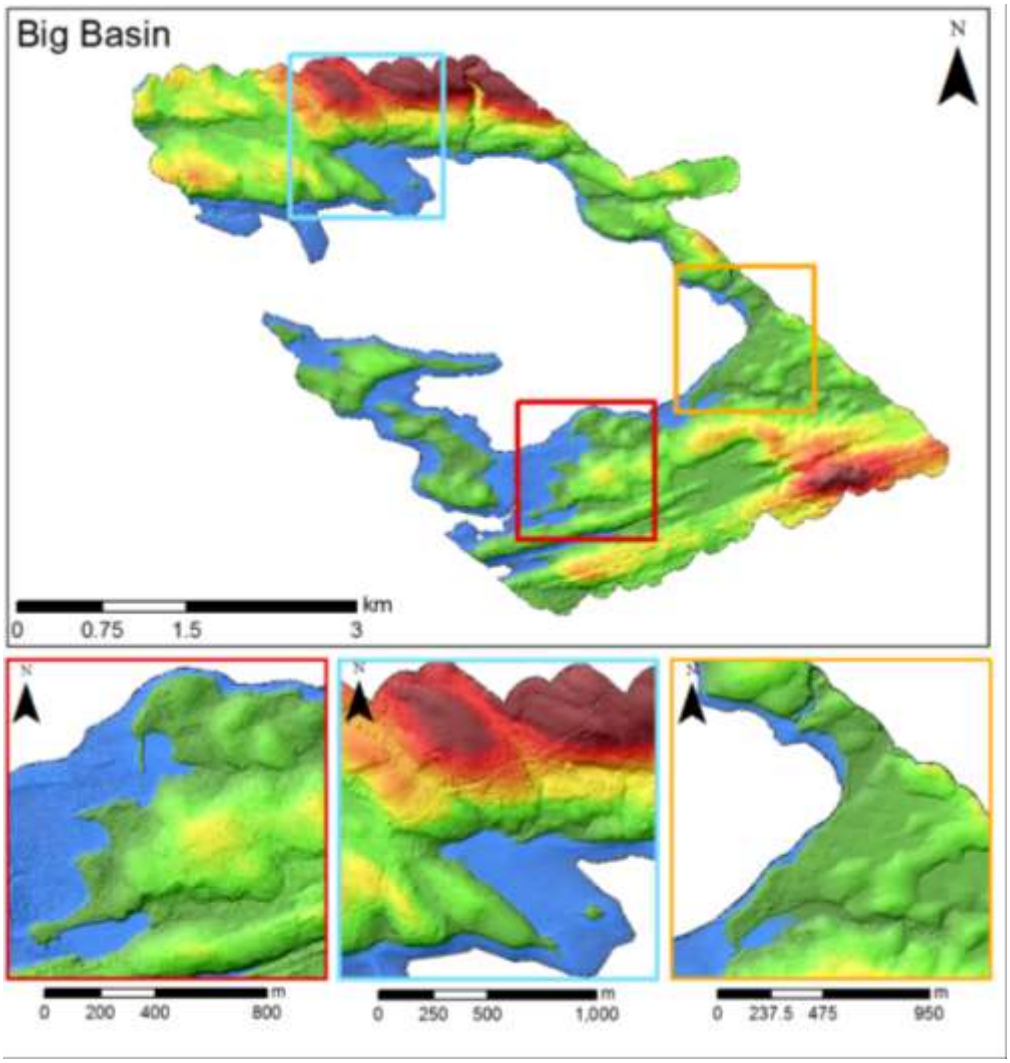


**Figure 3.5: Big Basin Colour Shaded Relief, with insets showing smaller features. Insets are matched to the larger figure by border colour.**

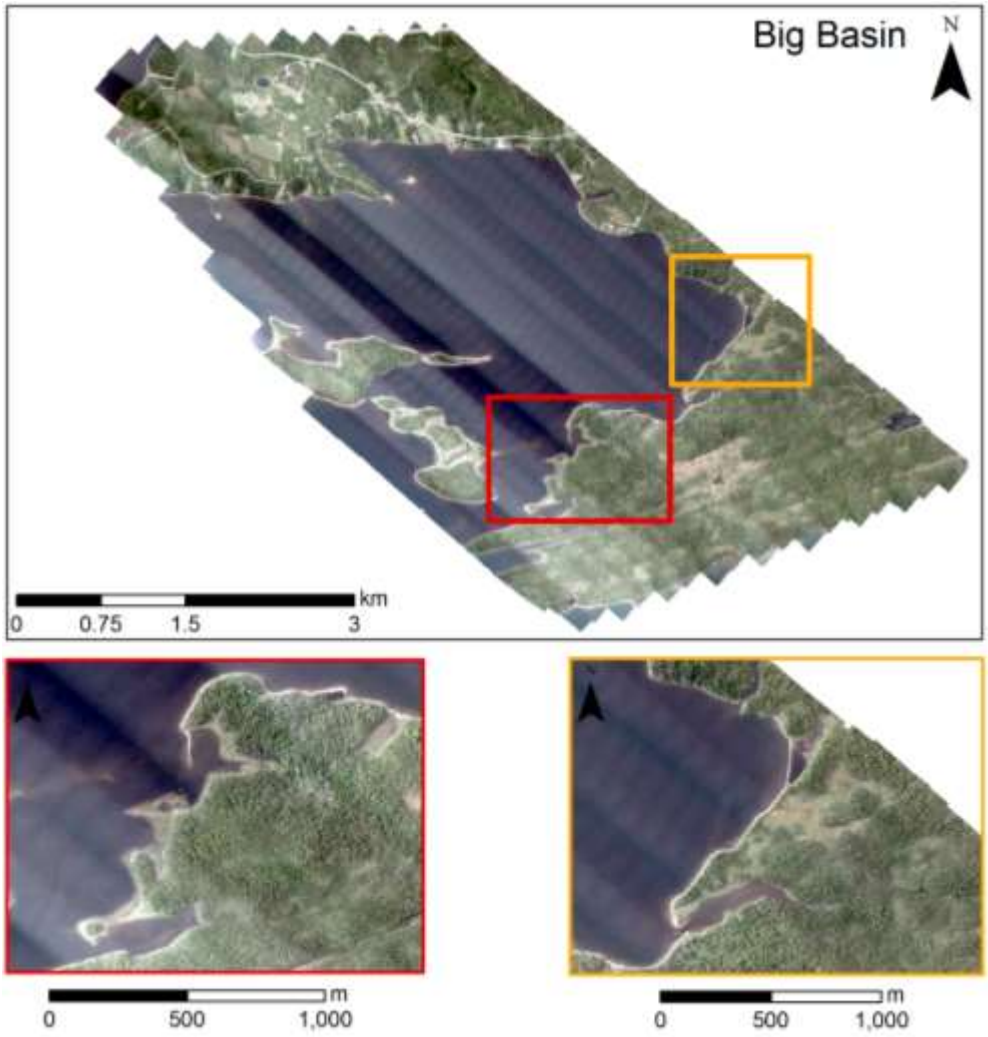


**Figure 3.6: Big Basin orthophoto mosaic, with insets showing smaller features. Insets are matched to the larger figure by border colour.**

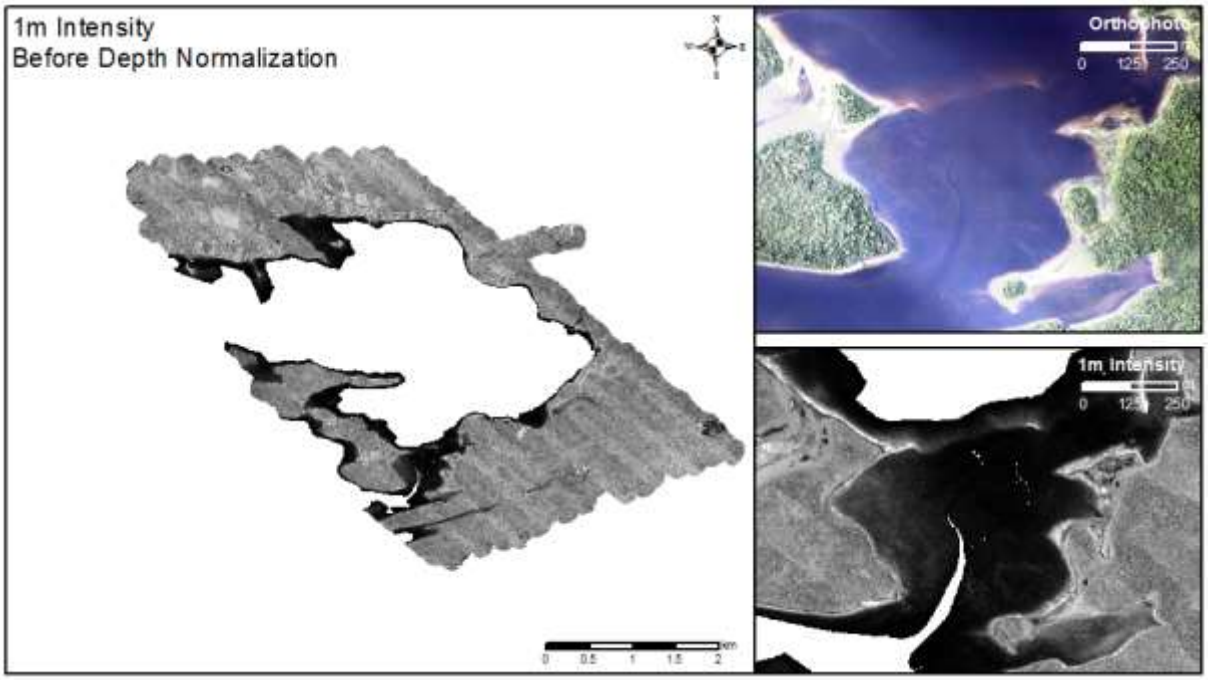


**Figure 3.7: Big Basin 1m intensity before depth normalization. Shown in inset map is orthophoto mosaic.**

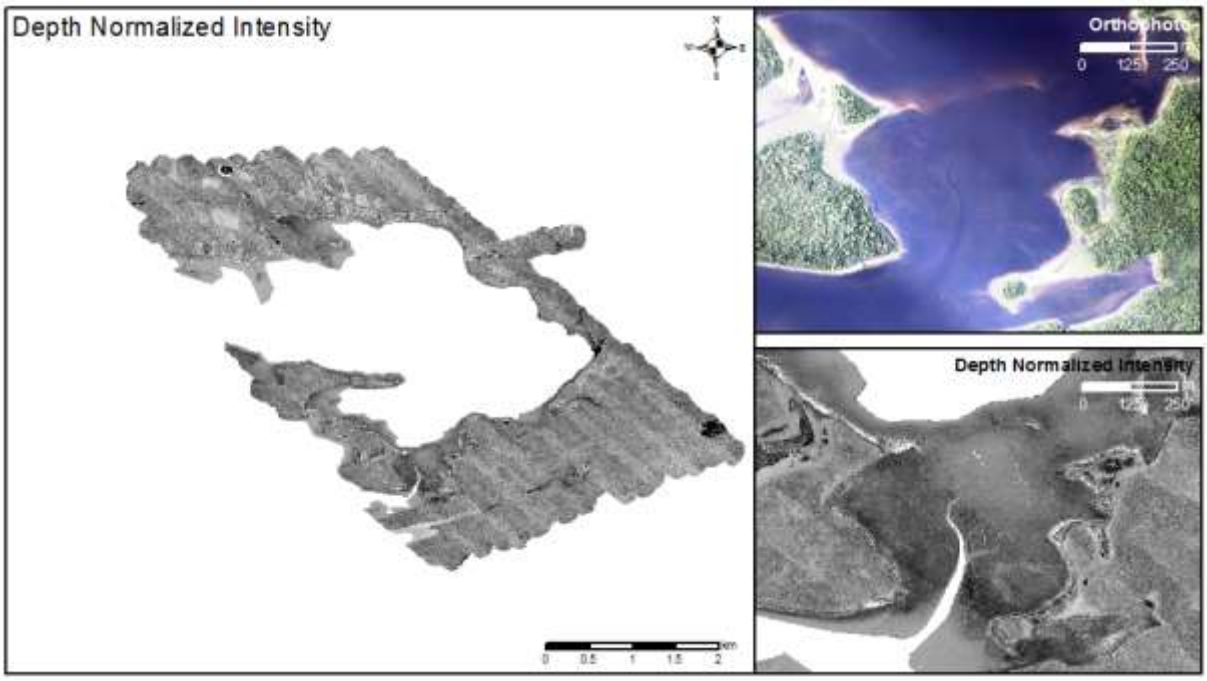


**Figure 3.8: Big Basin depth normalized intensity. Shown in inset map is orthophoto mosaic.**

### 3.2.2 Canso

The lidar survey at Canso penetrated to a minimum elevation of -14.91 m CGVD28 (Figure 3.9). The Digital Elevation Model (DEM) shows the topography relief in shades of green-yellow-red and the bathymetry relief in light blue. The CSR provides an exaggerated relief model and artificial shading to accentuate the topographic and bathymetric features in the DEM, making it useful for identifying the water and land boundary. The shades of darker blue represent deeper water. As a result, the CSR highlights the small islands throughout the area and the smaller panels matched by border colour provide a closer look at this (Figure 3.10). The orthophoto mosaic provides insights into land use, water clarity, bottom type, wave action, and river morphology (Figure 3.11). The details shown in the larger figure are highlighted in the panels at a larger scale, matched by border colour. The Canso orthophoto mosaic has shadows in the imagery due to the survey being flown later in the day.

The Depth Normalized Intensity model (DNI) can be a powerful tool to reveal submerged features and bottom type information that are challenging for the air photos to depict. The intensity data show the contrast between brightly coloured seabed and the dark colour of submerged vegetation. Prior to depth normalization, the inset pictured in Figure 3.12 appears dark, and it is difficult to interpret the seabed in both the 1m intensity and the air photo. The depth normalized intensity (Figure 3.13) provides additional context and reveals details in the intricate coves, such as the one pictured in the inset.

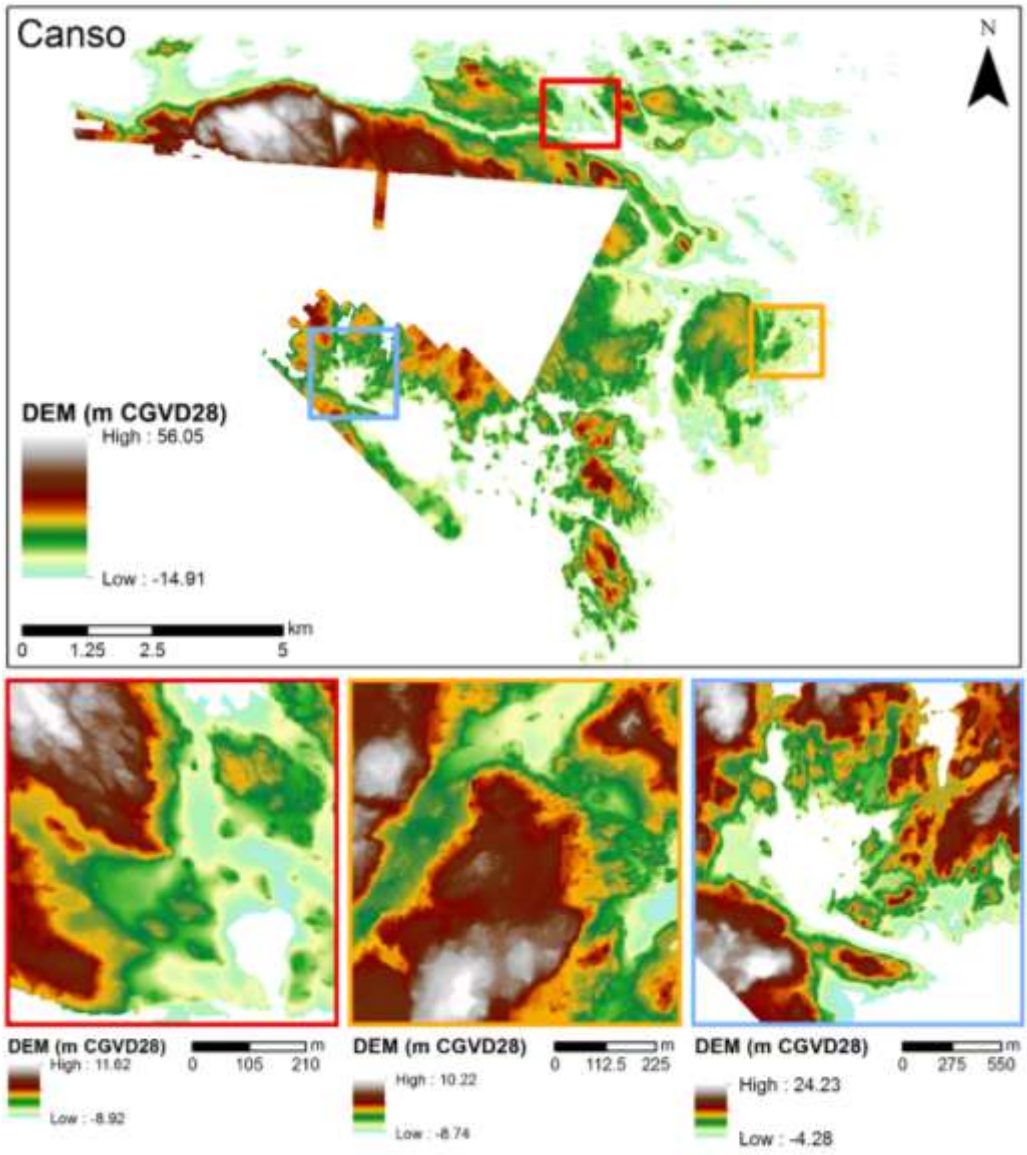


**Figure 3.9: Canso Digital Elevation Model, scaled to show bathymetry relief, and with insets showing smaller features. Insets are matched to the larger figure by border colour.**

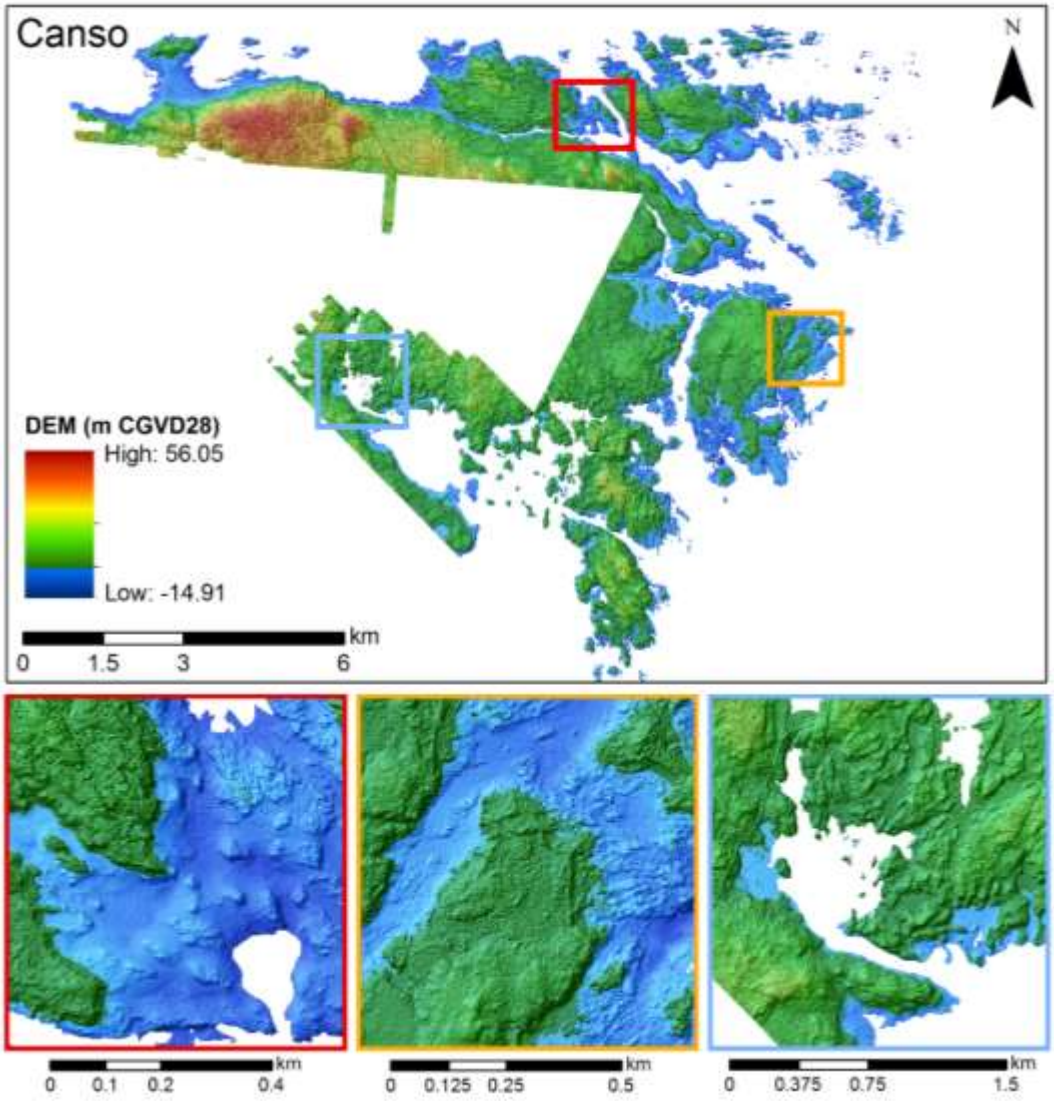


**Figure 3.10: Canso Colour Shaded Relief with insets showing smaller features. Insets are matched to the larger figure by border colour.**

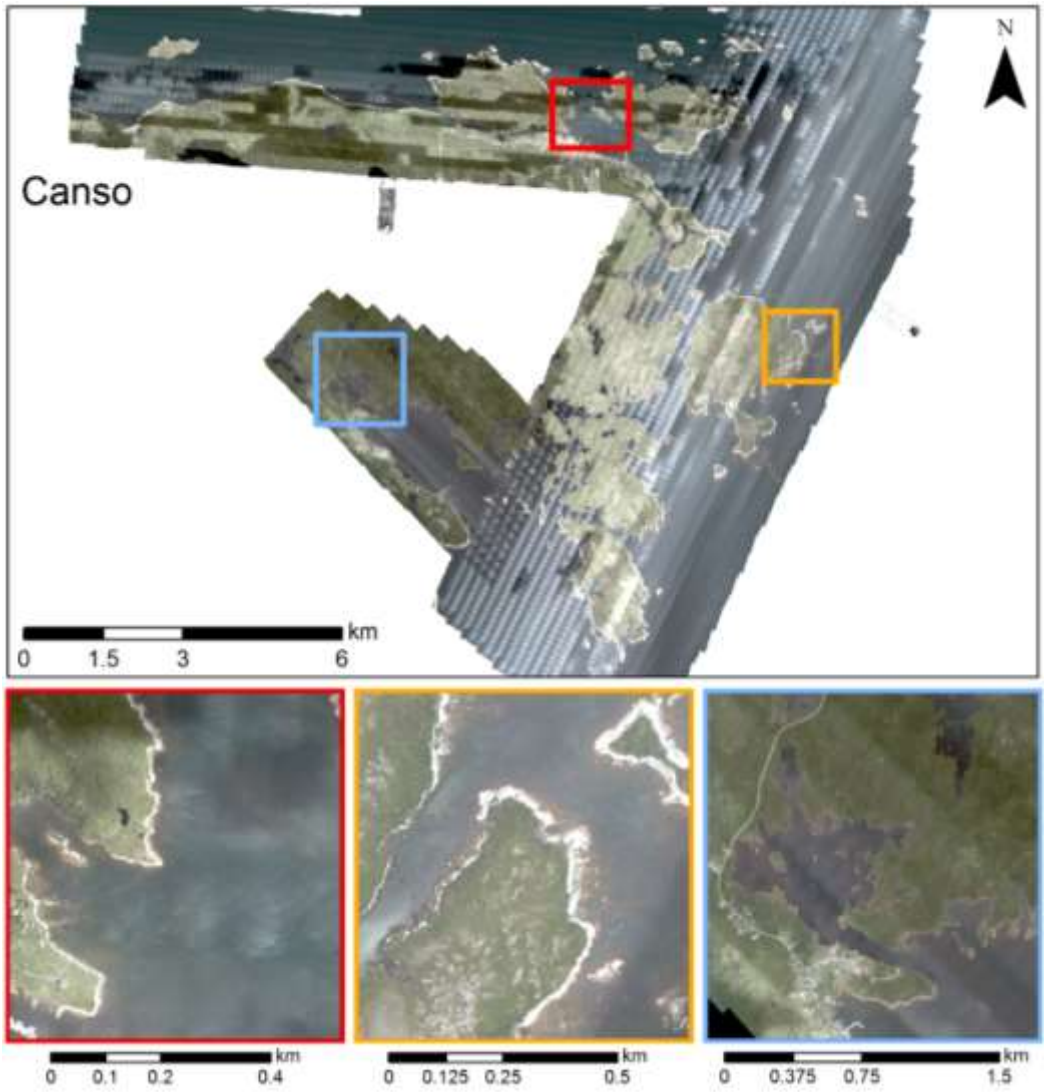


**Figure 3.11: Canso orthophoto mosaic, with insets showing smaller features. Insets are matched to the larger figure by border colour.**

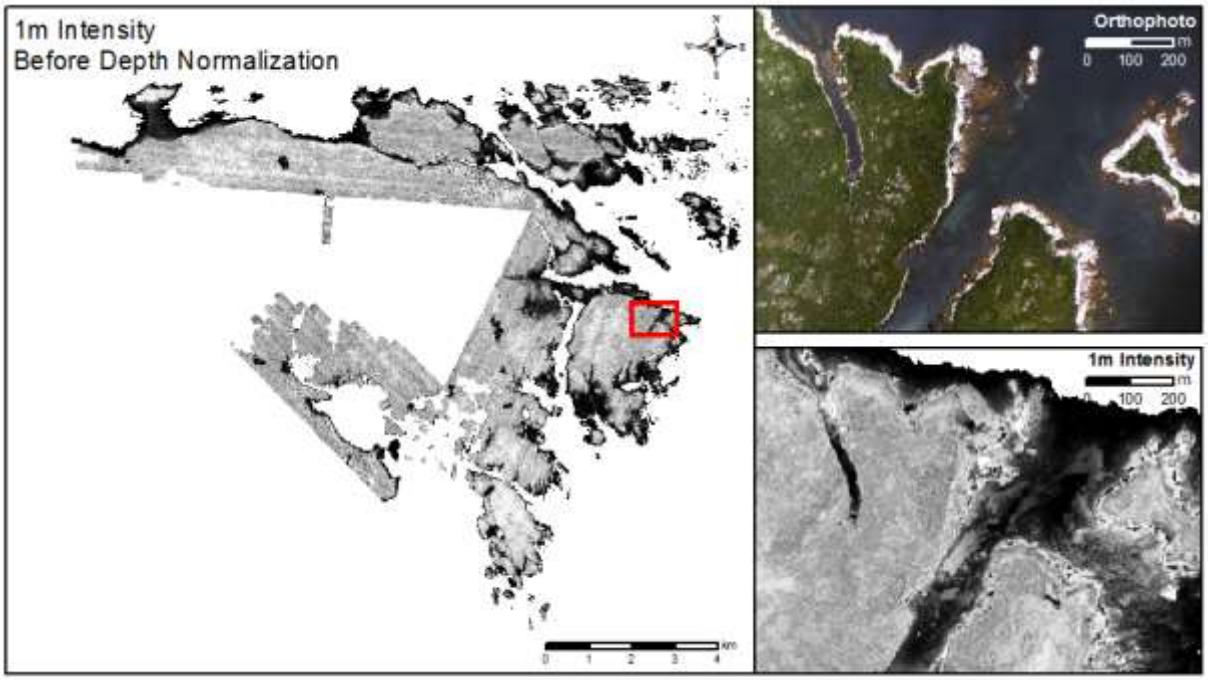


**Figure 3.12: Canso 1m intensity before depth normalization. Shown in inset map is orthophoto mosaic.**

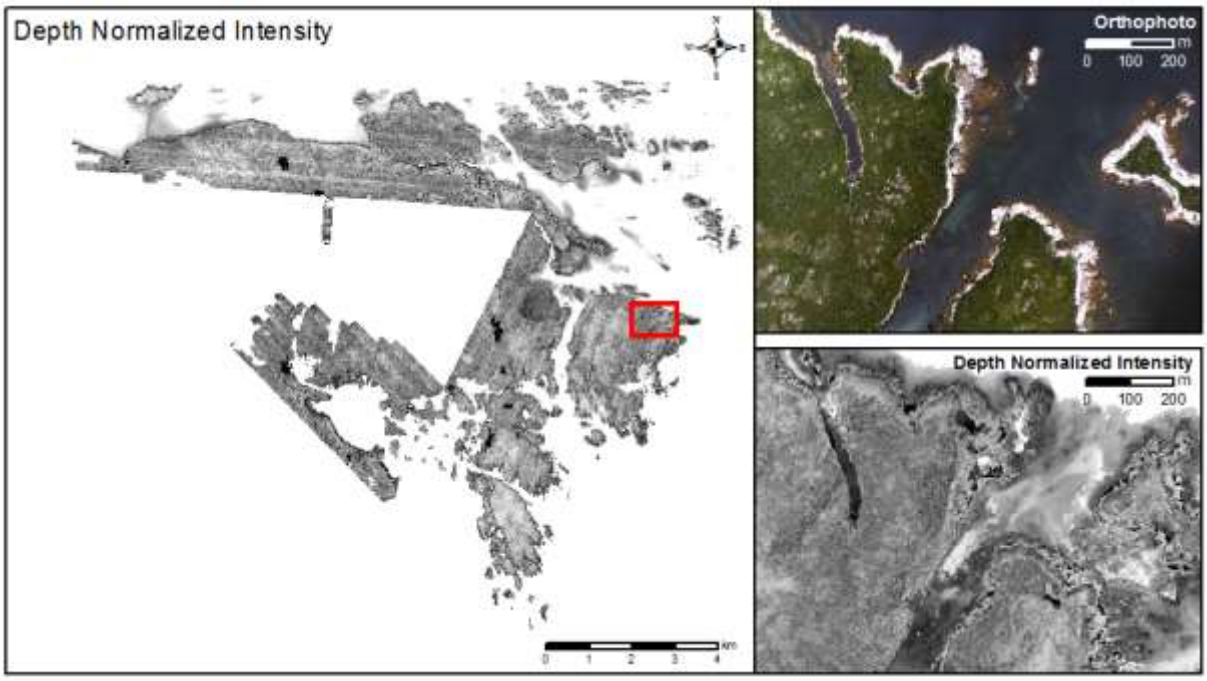


**Figure 3.13: Canso depth normalized intensity. Shown in inset map is orthophoto mosaic.**

### 3.2.3 Deer Island

The lidar survey at Deer Island successfully penetrated the majority of the seabed in the study area, the exception being the deeper part of the coastal area. This is where the Deer Island ferry route is located,

meaning there is deeper bathymetry and likely a channel in this location. The minimum elevation achieved by the lidar was -13.17 m CGVD28 (Figure 3.14). The CSR provides an exaggerated relief model and artificial shading to accentuate the topographic and bathymetric features in the DEM, making it useful for identifying the water and land boundary (Figure 3.15). The smaller panels highlight the details that cannot be seen in the larger figure, such as ripples and bumps around the smaller islands and coves. The orthophoto mosaic provides insights into land use, water clarity, bottom type, wave action, and river morphology (Figure 3.16). The Deer Island orthophoto mosaic has quite a bit of shadows in the Western half of the imagery due to the survey being flown later in the day. The Depth Normalized Intensity model (DNI) can be a powerful tool to reveal submerged features and bottom type information that are challenging for the air photos to depict. The intensity data show the contrast between brightly coloured seabed and the dark colour of submerged vegetation. Prior to depth normalization, the 1m intensity appears dark, making it difficult to interpret details on the seabed (Figure 3.17). The depth normalized intensity highlights the detail of the seabed, making it possible to depict the dark colour of submerged vegetation, particularly around the nearshore boundary pictured in Figure 3.18.

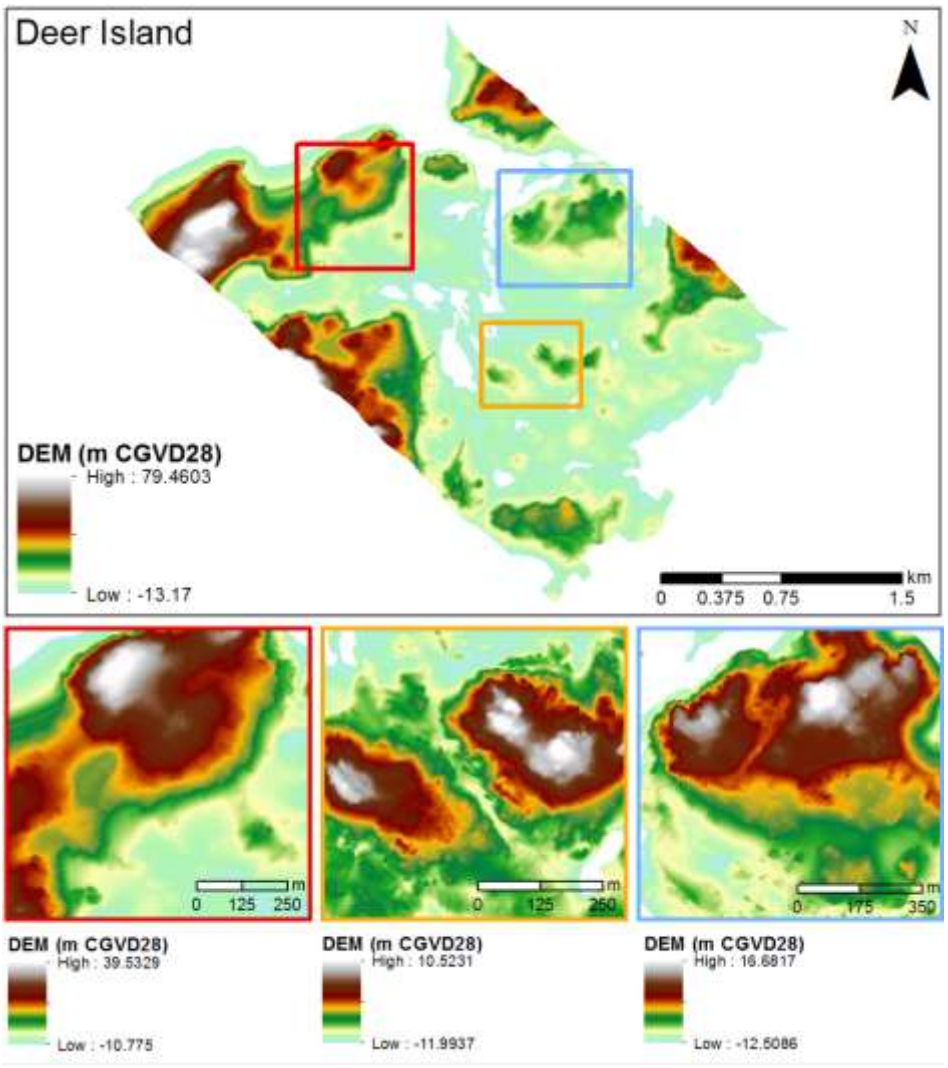


**Figure 3.14: Deer Island Digital Elevation Model, scaled to show bathymetry relief, and with insets showing smaller features. Insets are matched to the larger figure by border colour.**

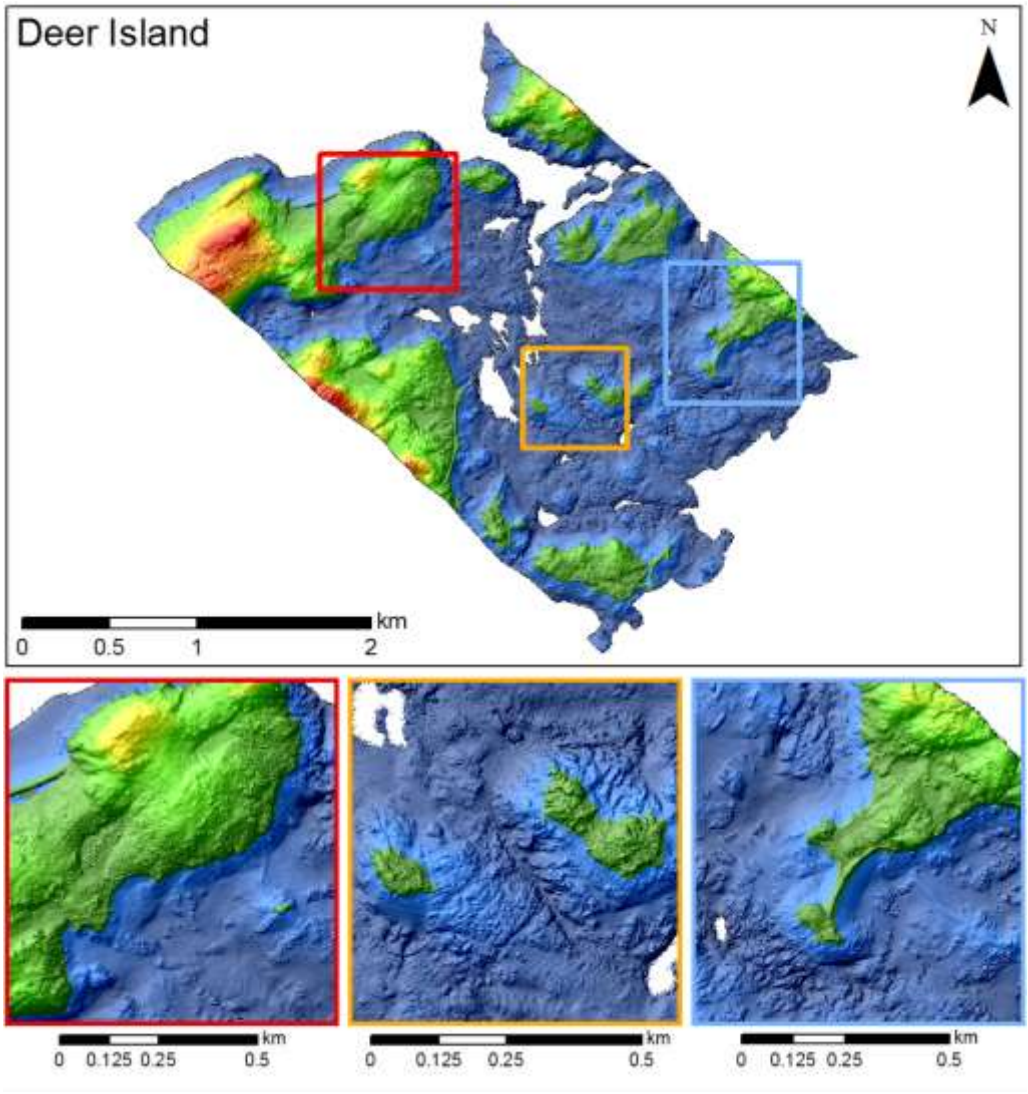


**Figure 3.15: Deer Island Colour Shaded Relief, with insets showing smaller features. Insets are matched to the larger figure by border colour.**

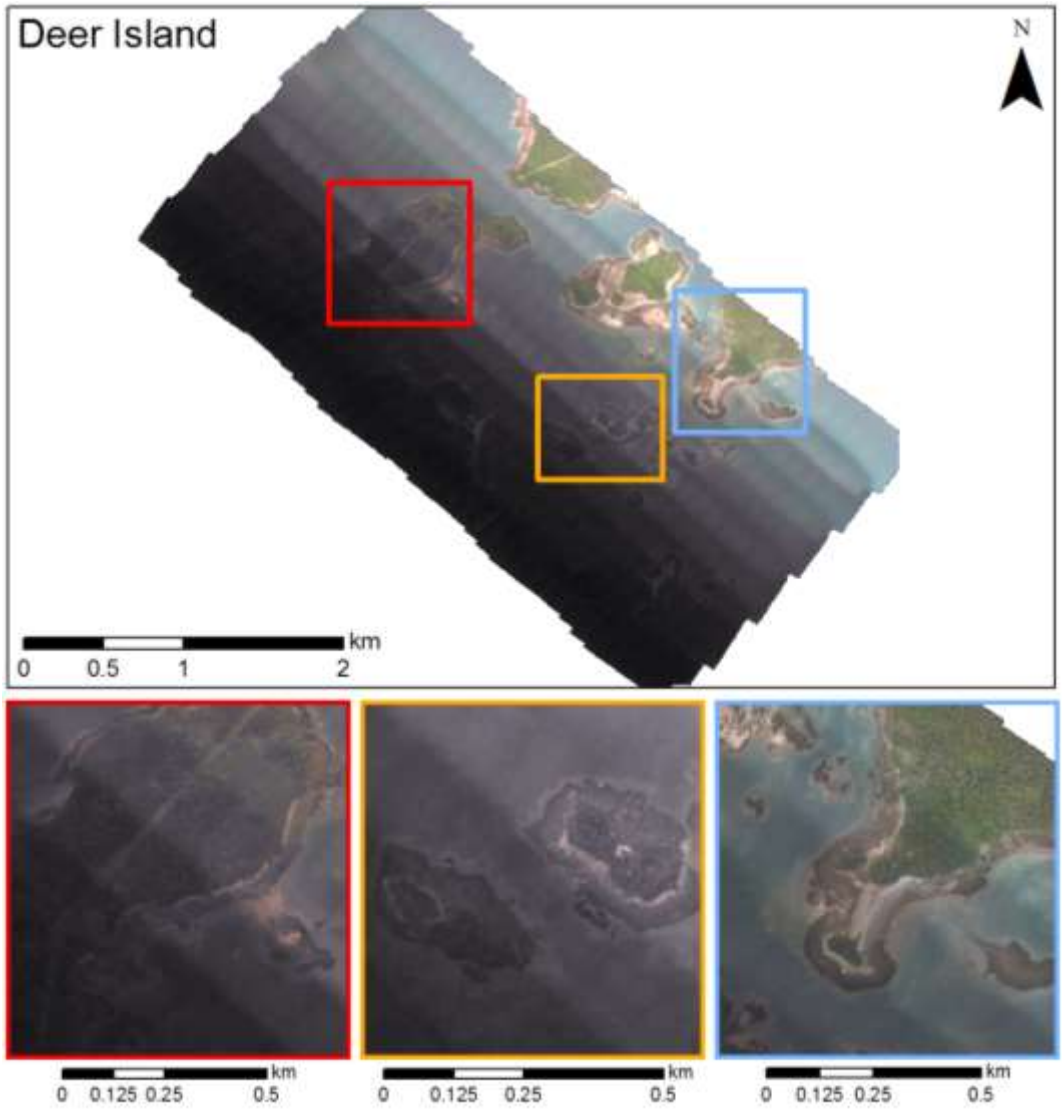


**Figure 3.16: Deer Island orthophoto mosaic, with insets showing smaller features. Insets are matched to the larger figure by border colour.**

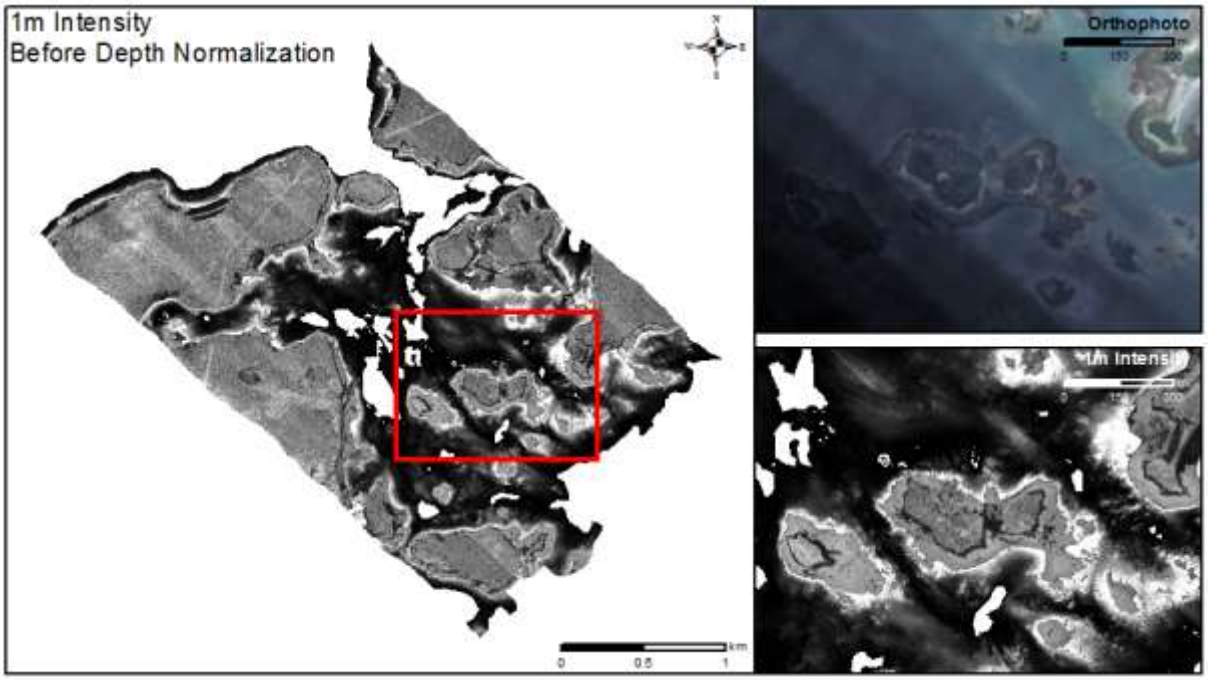


**Figure 3.17: Deer Island 1m intensity before depth normalization. Shown in inset map is orthophoto mosaic.**

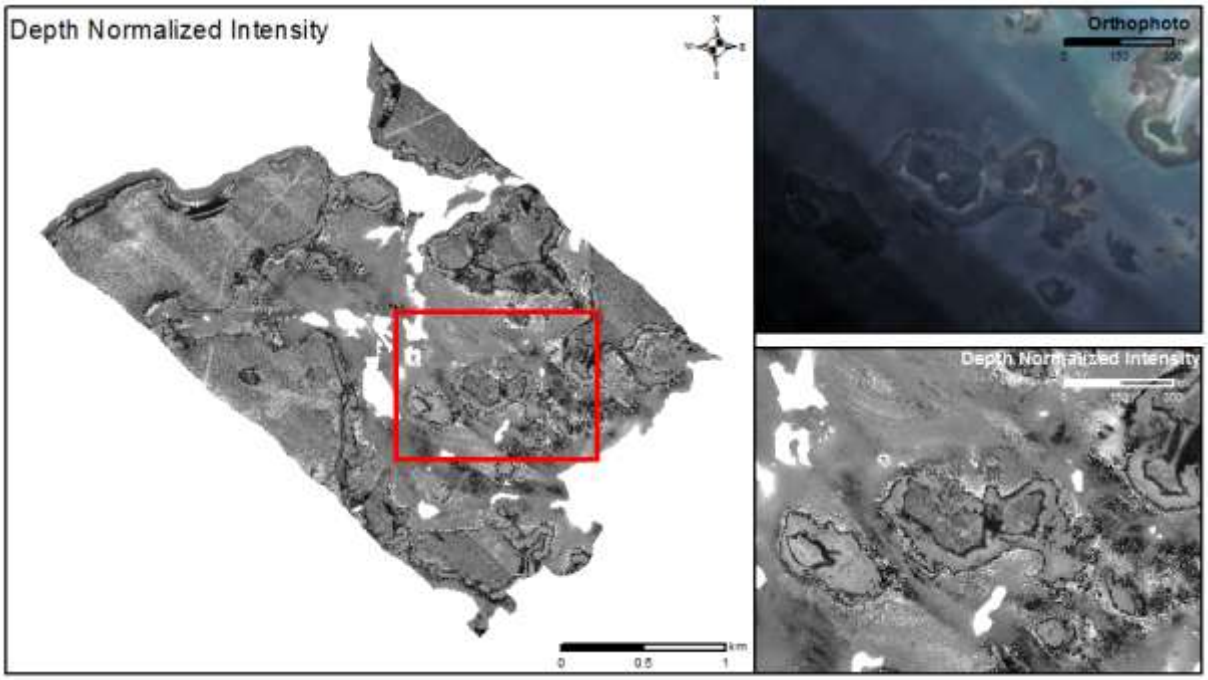


**Figure 3.18: Deer Island depth normalized intensity. Shown in inset map is orthophoto mosaic.**

### 3.2.4 Grand Manan

The lidar survey at Grand Manan penetrated to a minimum elevation of -11.35 m CGVD28. The majority of the minimum elevation values are located in the northern portion of the study area. The water in Grand Manan was clear and the bathymetry was quite deep with cliffs around the coastline, as can be interpreted in the DEM (Figure 3.19). The small blue inset frame in Figure 3.19 highlights one of the small islands shown in green, and the bathymetry shown in light blue. This symbology highlights where the land ends and the water begins. There is no gradual decrease in elevation, rather a cliff, highlighting the steep coastline in this study area. In addition to the DEM, the CSR is useful for identifying where the land ends, and the water begins, as it provides an exaggerated relief model and artificial shading to accentuate the topographic and bathymetric features in the DEM. The smaller panels in Figure 3.20 highlight the details that cannot be seen in the larger figure, such as channels and ridges that cannot be seen at the full scale extent.

The orthophoto mosaic provides insights into land use, water clarity, bottom type, wave action, and river morphology. There are some shadows in the Grand Manan orthophoto mosaic (Figure 3.21) due to the surveys being flown on separate days. The details that can be seen in the larger figure are highlighted in the smaller panels, matched by border colour. The Depth Normalized Intensity model (DNI) can be a powerful tool to reveal submerged features and bottom type information that are challenging for the air photos to depict. The intensity data show the contrast between brightly coloured seabed and the dark colour of submerged vegetation. Prior to depth normalization, the 1m intensity appears dark, making it difficult to interpret the reflectance of the seabed or submerged vegetation (Figure 3.22). The depth normalized intensity highlights the detail of the seabed, making it possible to depict the dark colour of submerged vegetation, just off the coast of the island as pictured in the inset in Figure 3.23.

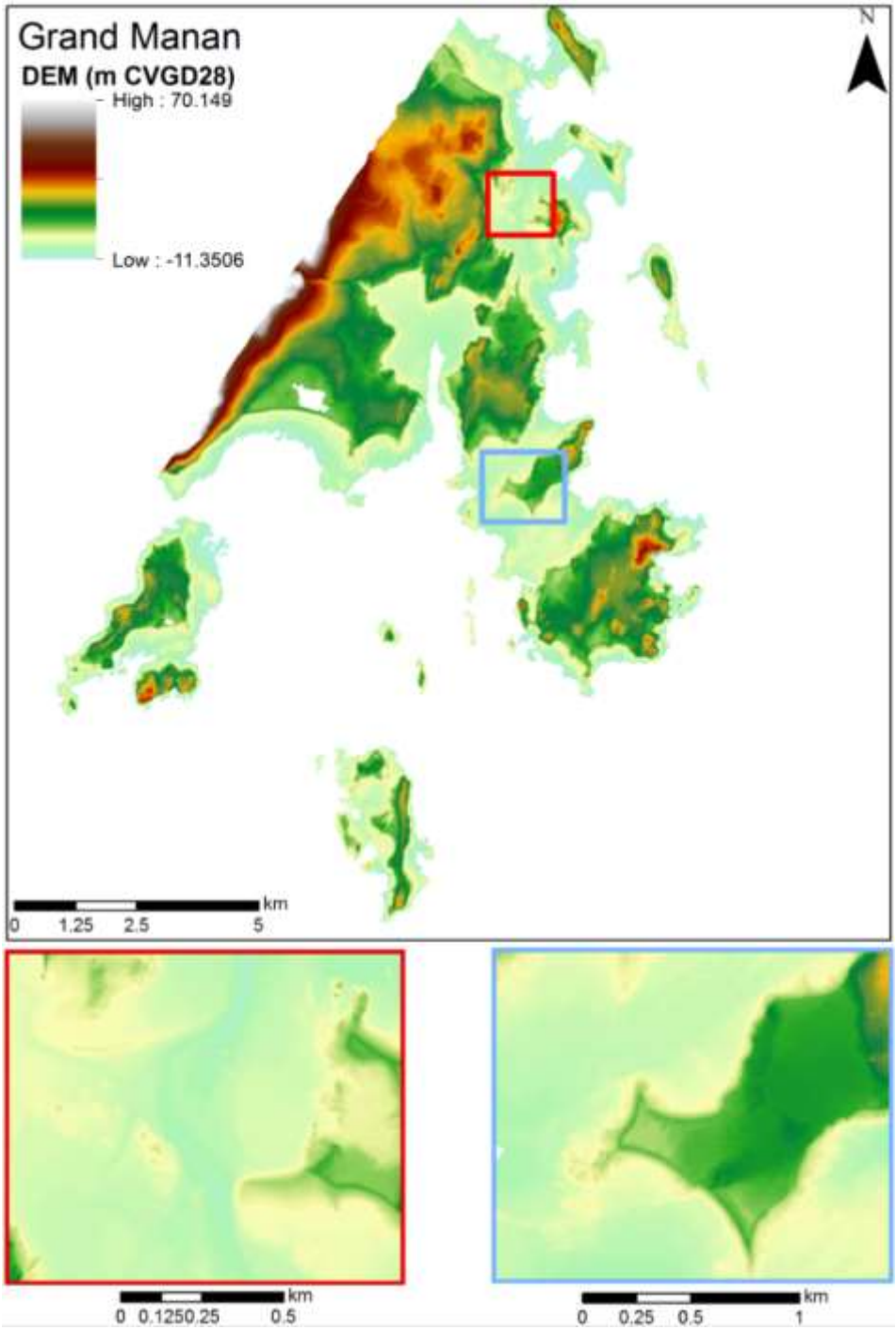


**Figure 3.19: Grand Manan Digital Elevation Model, scaled to show bathymetry relief, and with insets showing smaller features. Insets are matched to the larger figure by border colour.**

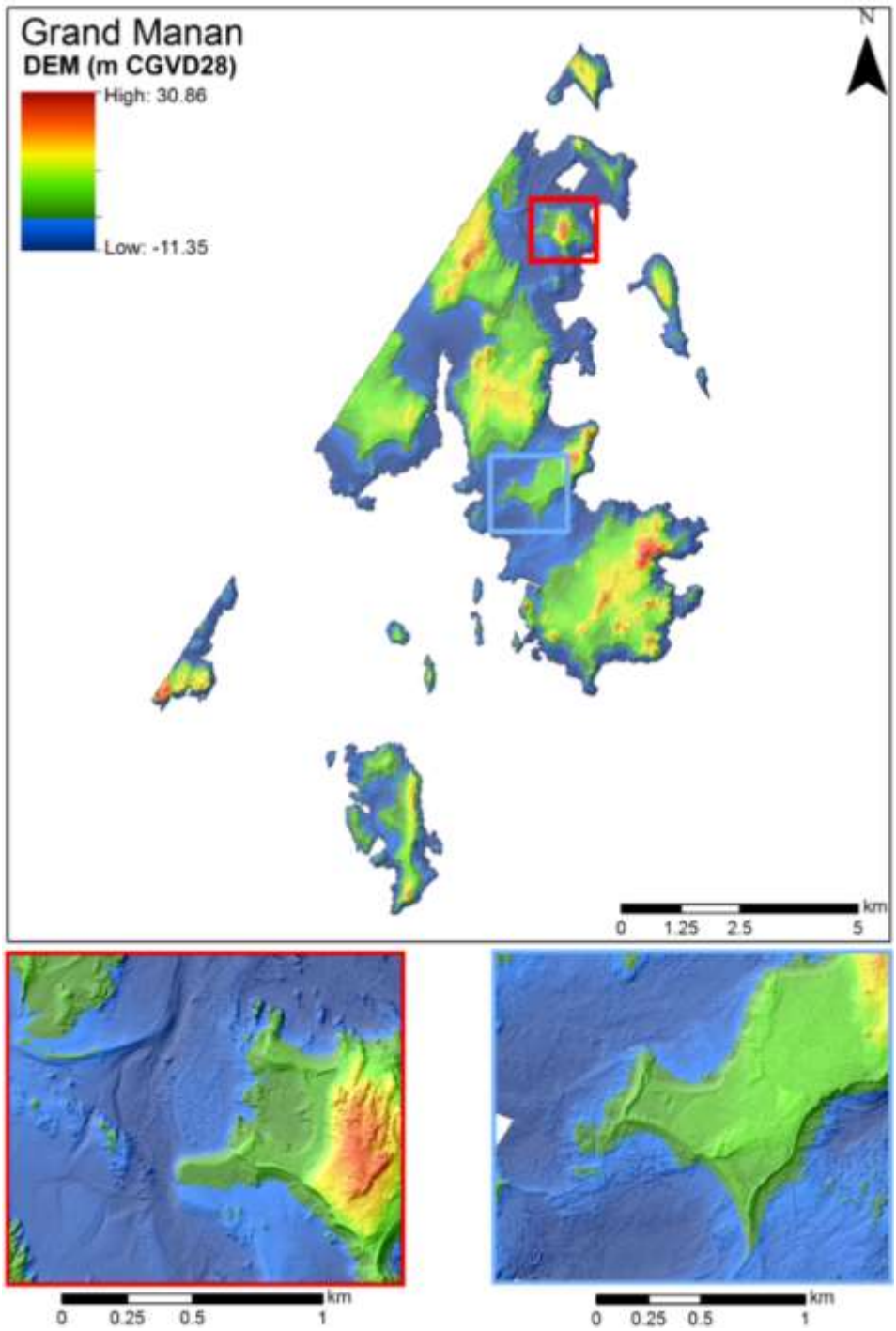


**Figure 3.20: Grand Manan Colour Shaded Relief, with insets showing smaller features. Insets are matched to the larger figure by border colour.**

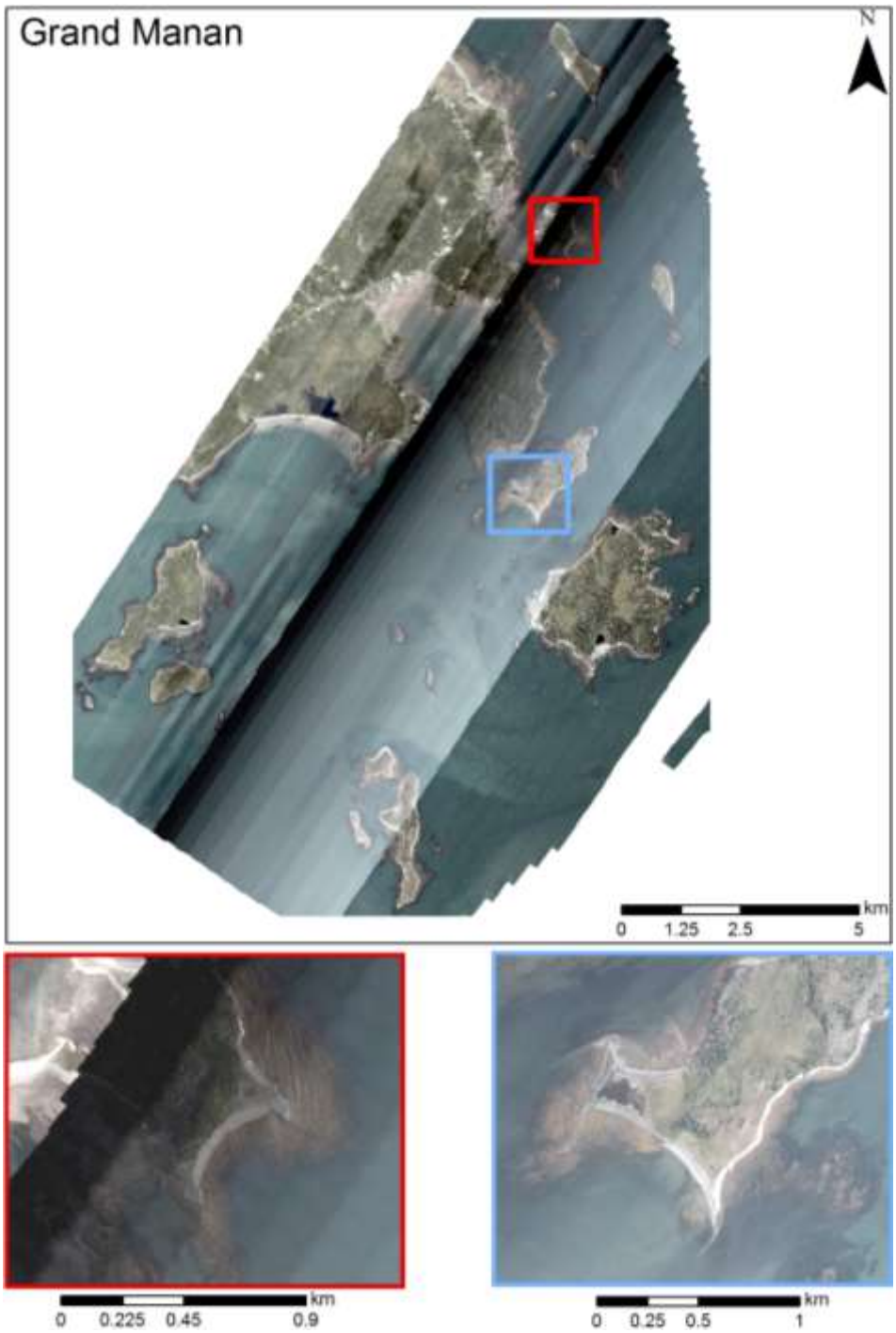


**Figure 3.21: Grand Manan orthophoto mosaic, with insets showing smaller features. Insets are matched to the larger figure by border colour.**

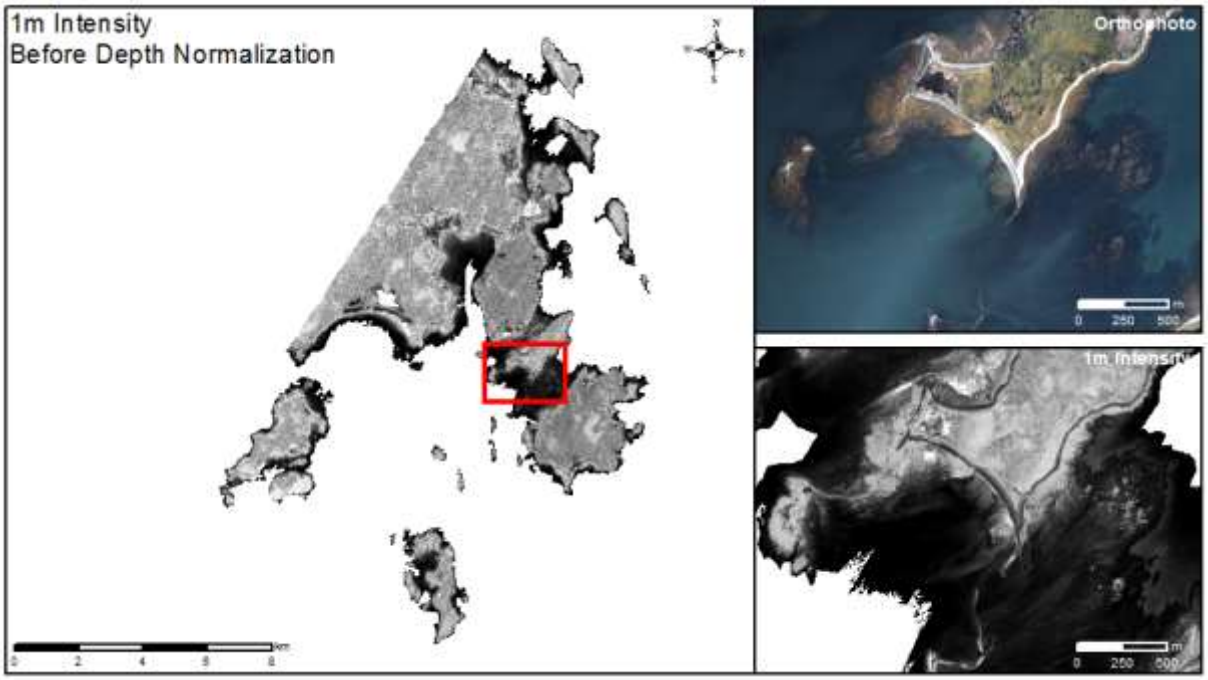


**Figure 3.22: Grand Manan 1m intensity before depth normalization. Shown in inset map is orthophoto mosaic.**

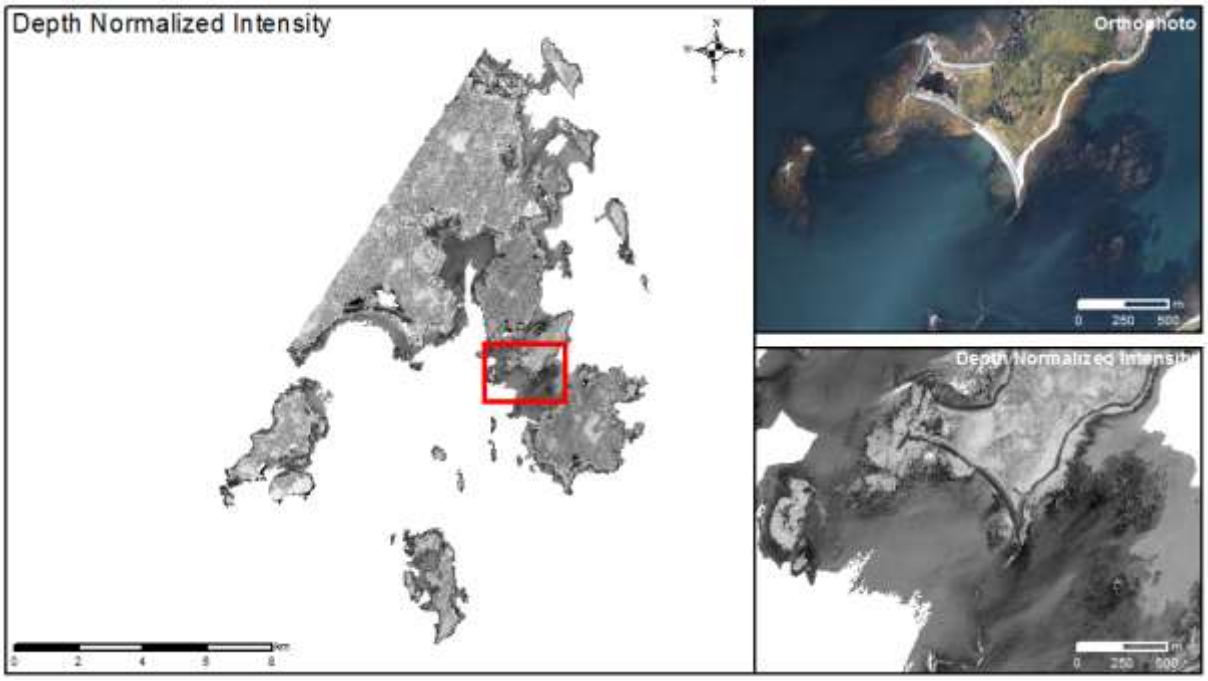


**Figure 3.23: Grand Manan depth normalized intensity. Shown in inset map is orthophoto mosaic.**

## 3.3 Ground Truth Maps

As indicated in Section 2.3, AGRG researchers conducted ground truth data collection in Canso and Big Basin. This included hard surface validation and depth measurements to validate the lidar, Secchi depth measurements for information on water clarity, and underwater photographs. The underwater photographs taken using a GoPro camera mounted to a quadrat are useful indicators of bottom type throughout the study area, particularly when these bottom photos can be spatially linked to the GPS points acquired during the ground truth collection. The following sections present some of the images obtained at Big Basin and Canso during the field season displayed on the RCD30 5 cm resolution orthophoto mosaics.

### 3.3.1 Big Basin

The bottom type at Big Basin was a combination of mud with some eelgrass. The water throughout the basin for the most part was dark and murky, consistent with the lidar, which did not penetrate the seabed in the basin. There was some clear water in the southeastern area of the basin where healthy eelgrass was also present. The following maps will highlight the field of view cover type (Figure 3.24) present throughout the survey. Maps also include water clarity during the survey.

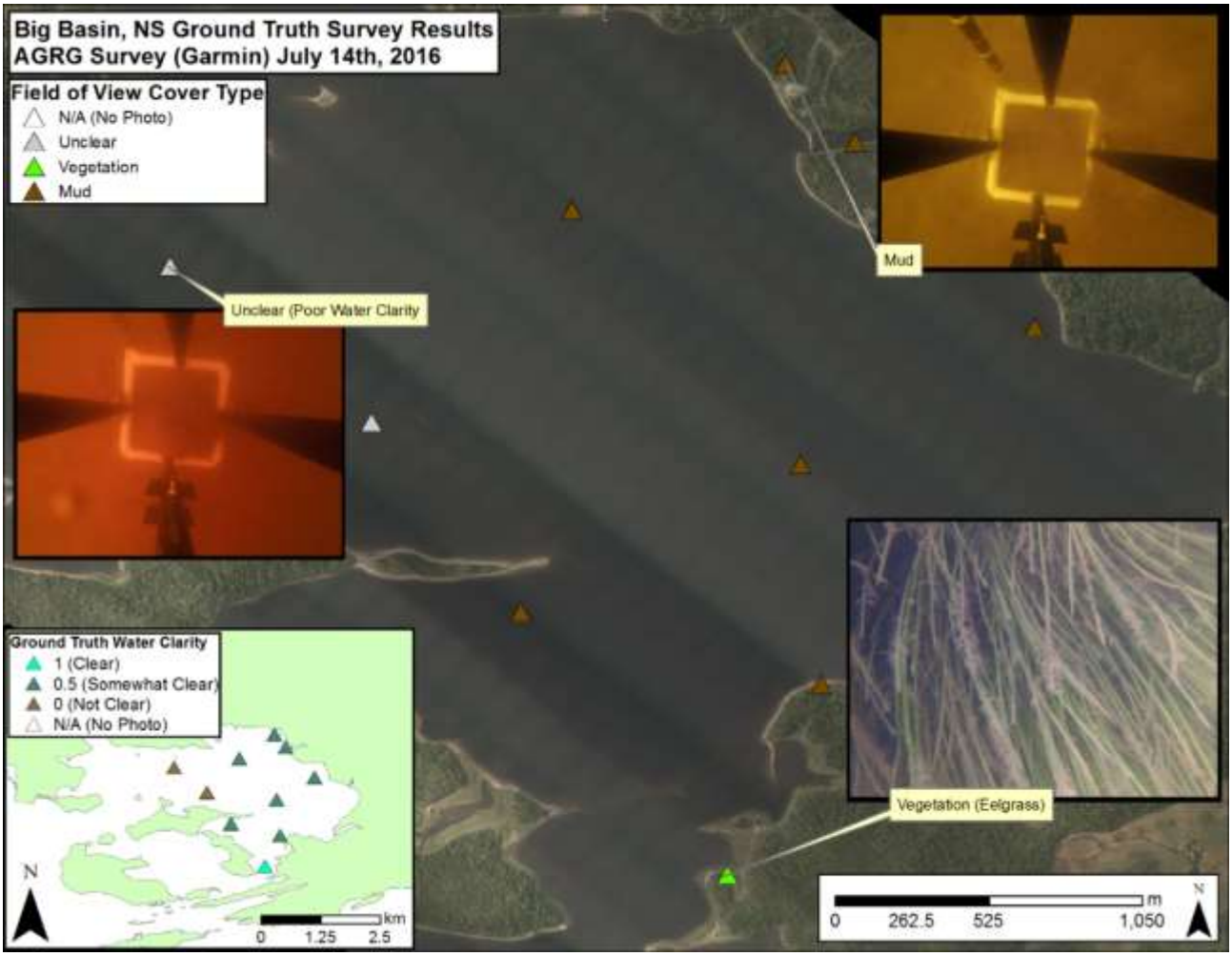


**Figure 3.24: Big Basin underwater photo ground truth for the July 14 survey symbolized to show the field of view cover type. Background image is RCD30 orthophoto RGB mosaic.**

### 3.3.2 Canso

The bottom type at Canso was a combination of vegetation and sand with a small amount of mud. The water was mainly very clear with the exception of two areas in the southwestern region of the study area nestled between islands. This is where mud was present. The following maps will highlight the field of view cover type (Figure 3.25, Figure 3.26) present throughout both ground truth surveys on July 20. Maps also include water clarity during the surveys.

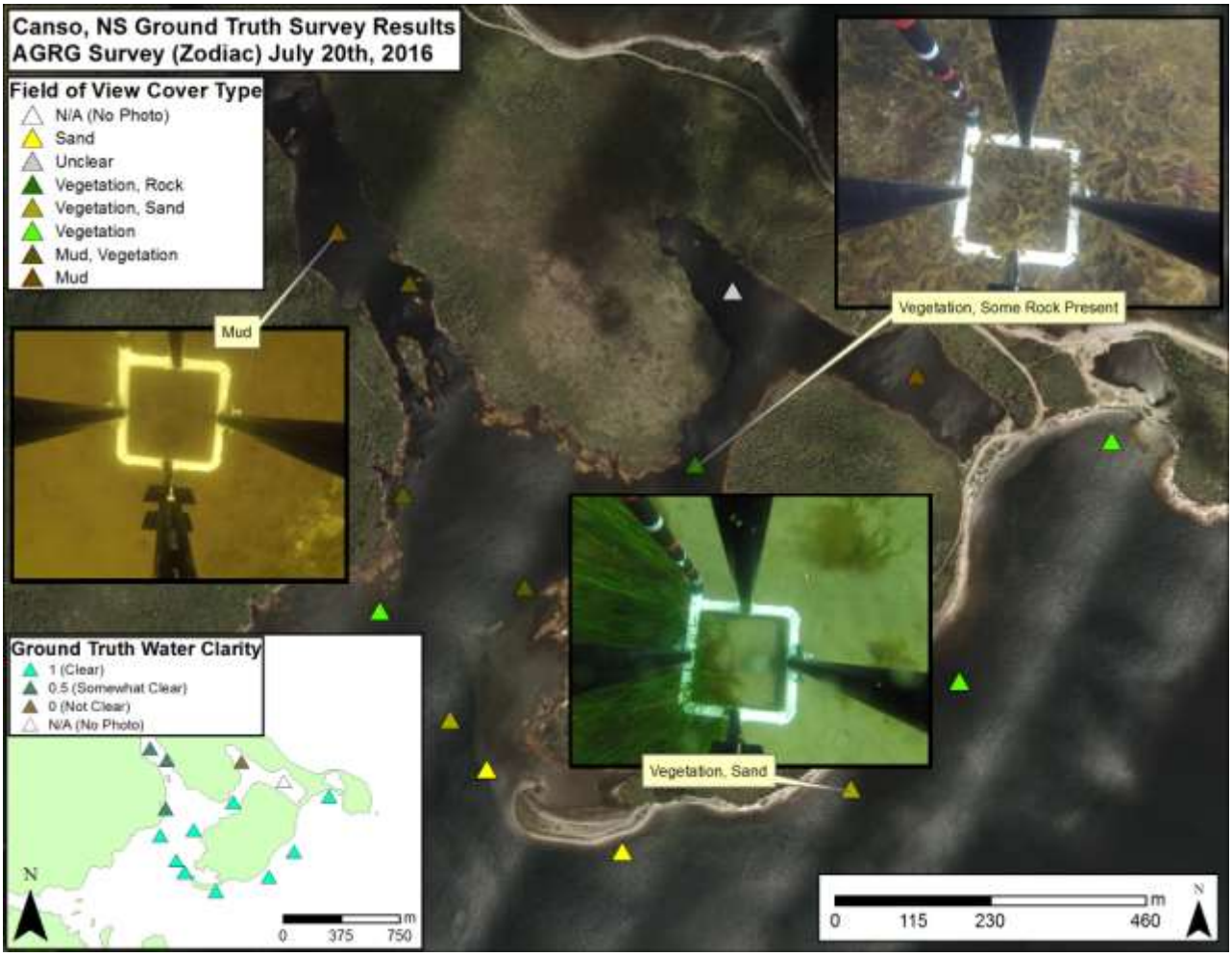


**Figure 3.25: Canso underwater photo ground truth for the July 20 survey (AGRG Zodiac) symbolized to show the field of view cover type. Background image is RCD30 orthophoto RGB mosaic.**

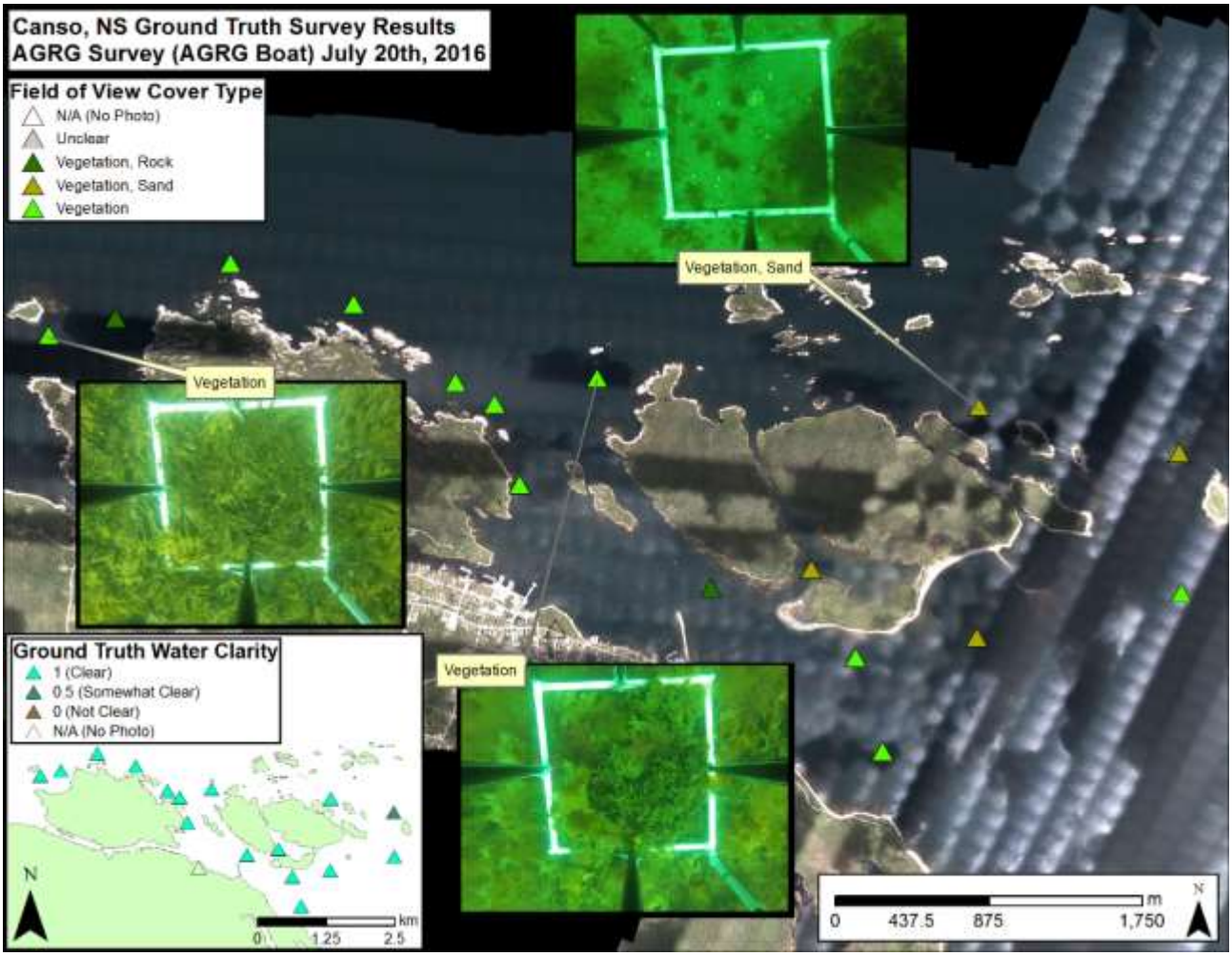


**Figure 3.26: Canso underwater photo ground truth for the July 20 survey (AGRG aluminum boat) symbolized to show the field of view cover type.**

## 3.4 Bottom Type Classification and SAV Results

As described in Section 2.7 to Section 2.9, bottom type classification maps were produced for Big Basin, Canso, and Grand Manan. SAV maps were also derived. The following sections will present the results of the bottom classification, classes used, as well as the results of the SAV maps.

### 3.4.1 Big Basin

The bottom classification in Big Basin resulted in a primary cover type of submerged aquatic vegetation and sand in the southern portion of the study area. This is highlighted in the inset pictured in Figure 3.27. In the northern portion of the study area, the primary cover type was sand and submerged aquatic vegetation; sand. There was also some rock and gravel close to the nearshore area. The classes used in this bottom classification are shown in Table 3.1. Figure 3.28 compares the results of the bottom classification with the results of the ground truth collection to determine the agreement. There was a 100% bottom type agreement with the classification results and ground truth results.

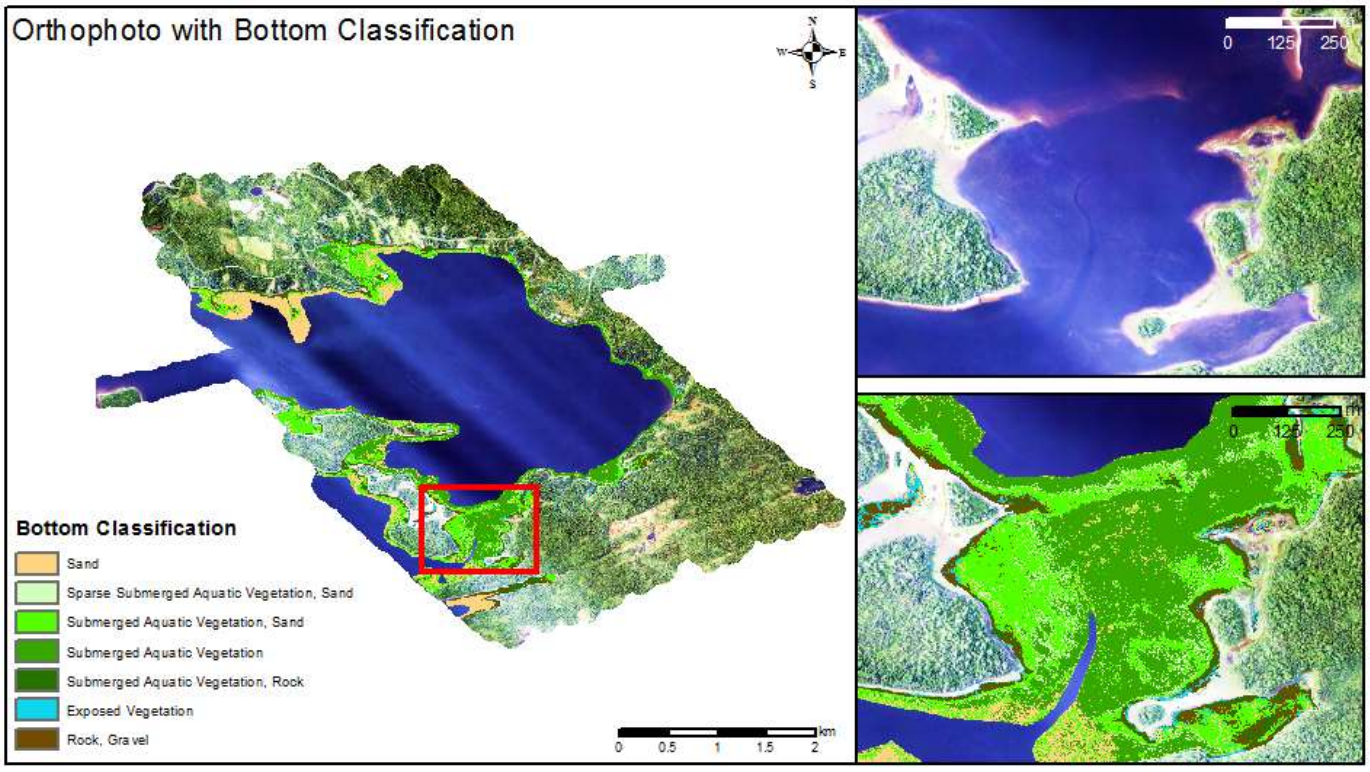


**Figure 3.27: Big Basin bottom classification with orthophoto mosaic.**

| Value | Bottom Type |
|---|---|
| 1 | Sand |
| 2 | Sparse Submerged Aquatic Vegetation; Sand |
| 3 | Submerged Aquatic Vegetation; Sand |
| 4 | Submerged Aquatic Vegetation |
| 5 | Submerged Aquatic Vegetation; Rock |
| 6 | Exposed Vegetation |
| 7 | Rock; Gravel |

**Table 3.1: Classes used in Big Basin bottom classification.**

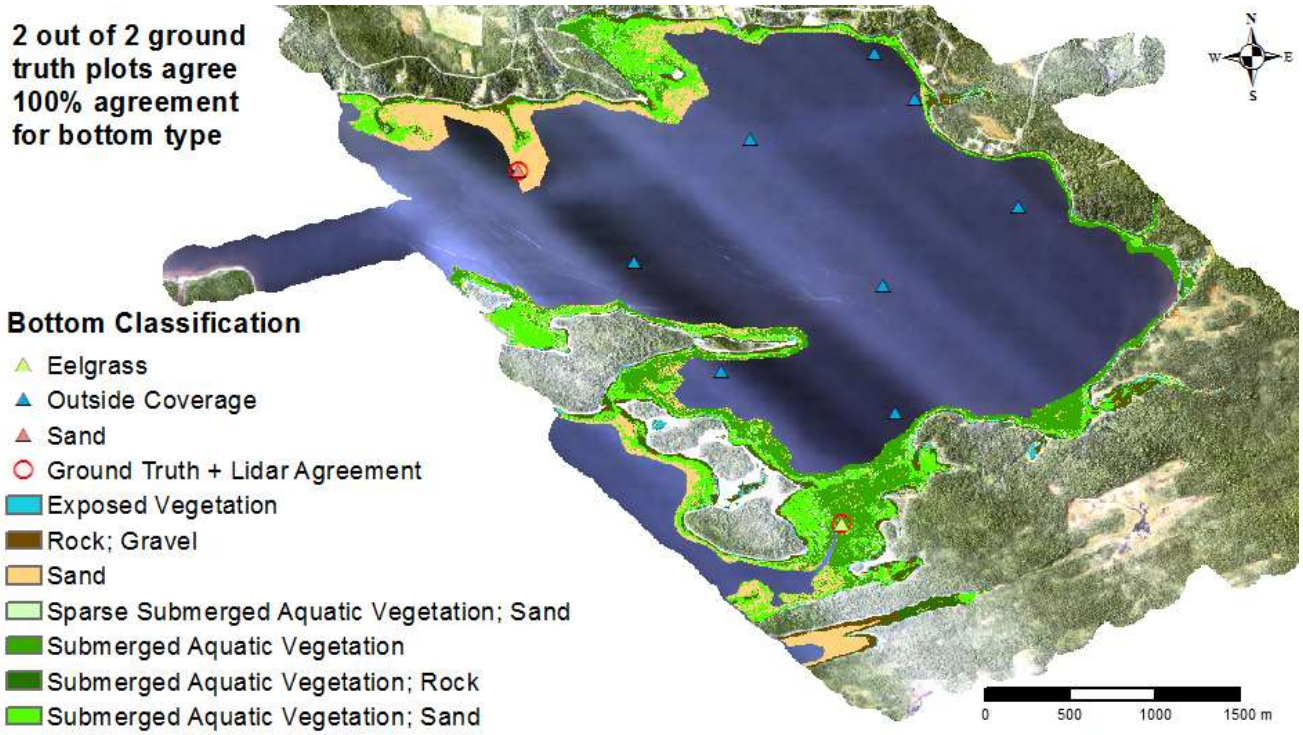


**Figure 3.28: Big Basin bottom classification map shown with validation results of ground truth collection.**

Figure 3.29 highlights the results of the SAV map for Big Basin. Comparable to the results of the bottom classification, the majority of the submerged aquatic vegetation is in the southern portion of the study area.

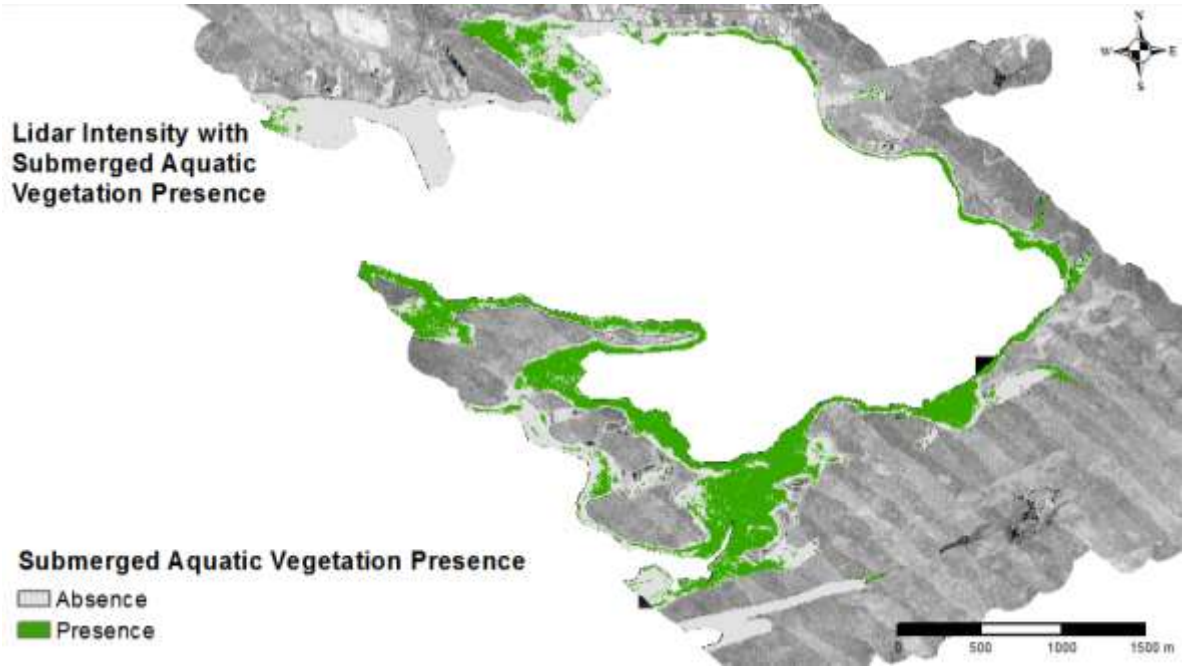


**Figure 3.29: Big Basin submerged aquatic vegetation map showing presence of vegetation in green and absence in grey.**

### 3.4.2 Canso

The bottom classification in Canso resulted in a primary cover type of vegetation, specifically kelp, moss, and seaweed. This is highlighted in the inset pictured in Figure 3.30 in the eastern and northeastern areas of Canso. Additionally, there was a large amount of deep sand/mud in the northern areas of Canso, while most of the shallow sand/rock/rockweed was found in the sheltered areas in the center of the study area. The classes used in this bottom classification are shown in Table 3.2. Figure 3.31 compares the results of the bottom classification with the results of the ground truth collection to determine the agreement. There was a 73.6% bottom agreement with the classification results and ground truth results.

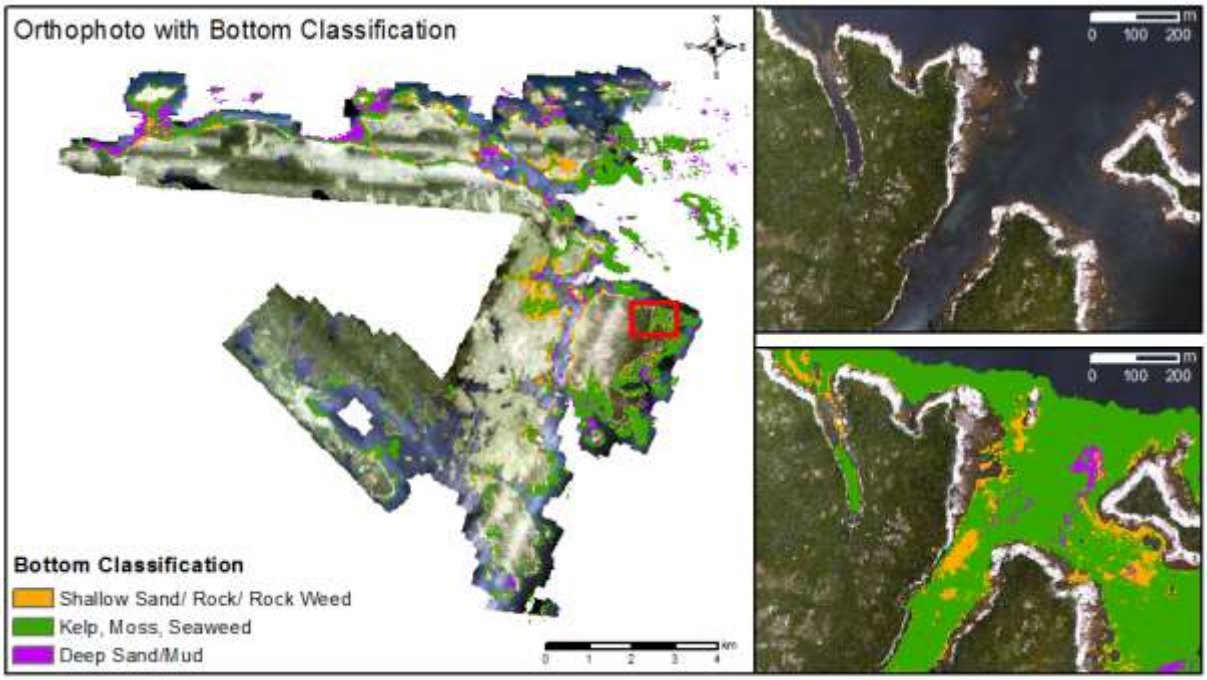


**Figure 3.30: Canso bottom classification with orthophoto mosaic.**

| Value | Bottom Type |
|---|---|
| 1 | Kelp, Moss, Seaweed |
| 2 | Deep Sand/Mud |
| 3 | Shallow |

**Table 3.2: Classes used in Canso bottom classification.**

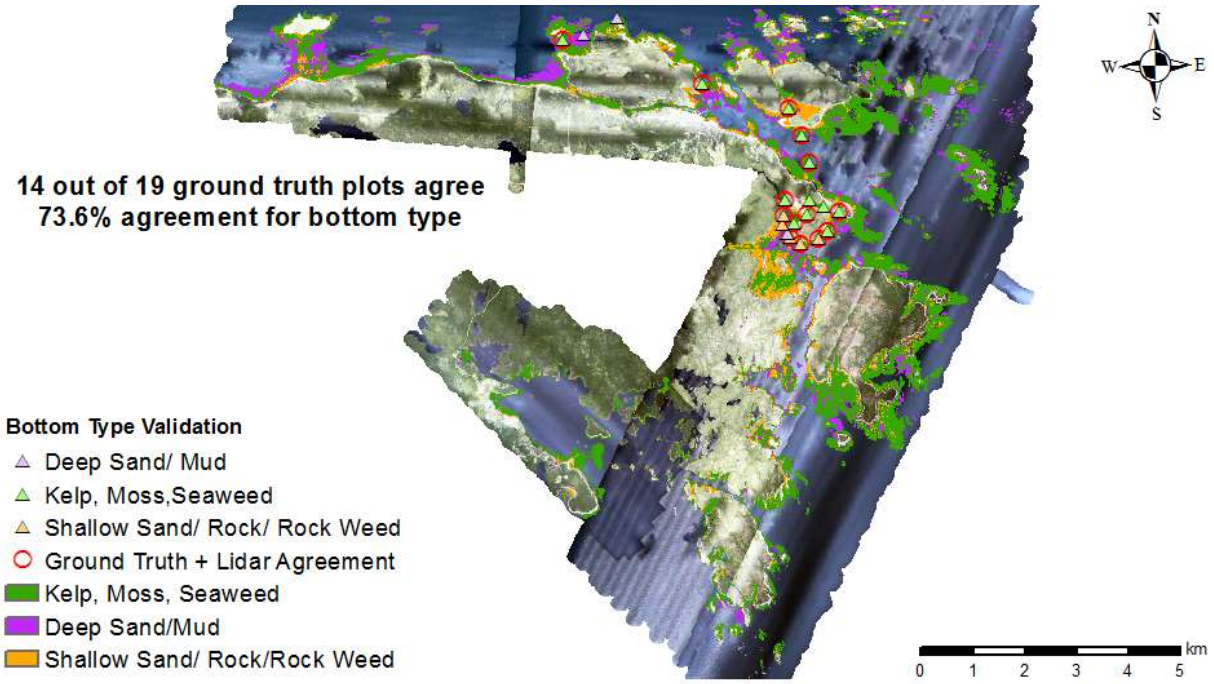


**Figure 3.31: Canso bottom classification map shown with validation results of ground truth collection.**

Figure 3.32 highlights the results of the SAV map for Canso. Comparable to the results of the bottom classification, the majority of the submerged aquatic vegetation is in the eastern and northeastern areas.

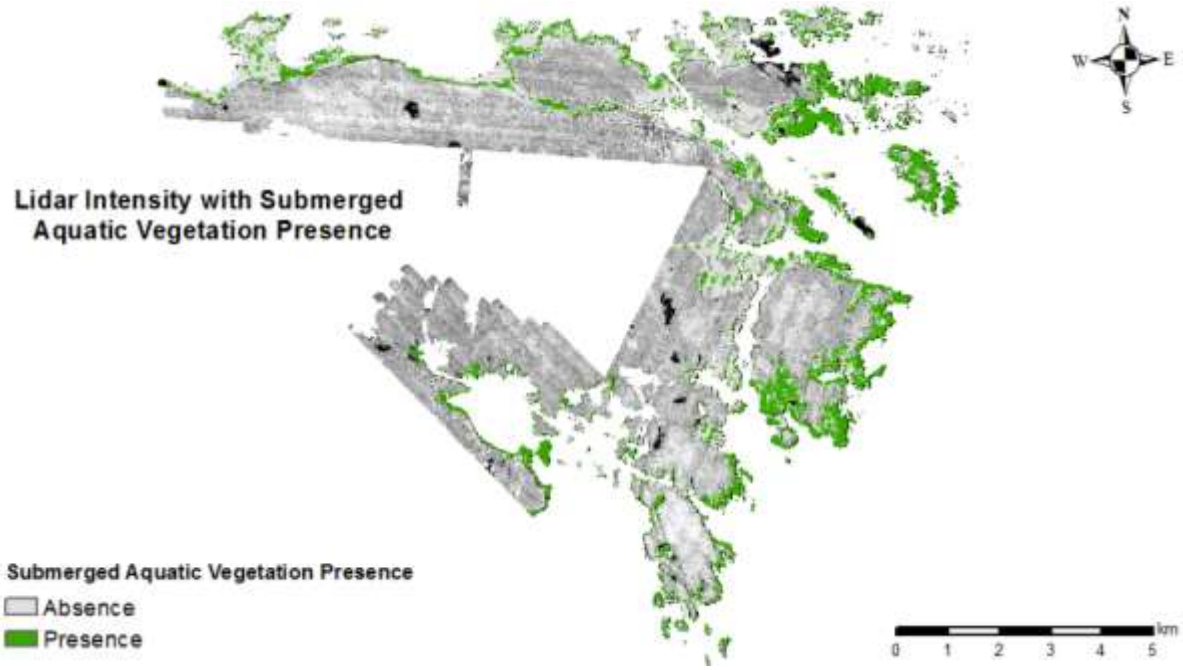


**Figure 3.32: Canso submerged aquatic vegetation map showing presence of vegetation in green and absence in grey.**

### 3.4.3 Grand Manan

The bottom classification in Grand Manan resulted in a primary cover type of submerged aquatic vegetation. The classification also resulted in a large amount of sand around the coastline of the island. This is highlighted in the inset pictured in Figure 3.33. The classes used in this bottom classification are shown in Table 3.3.

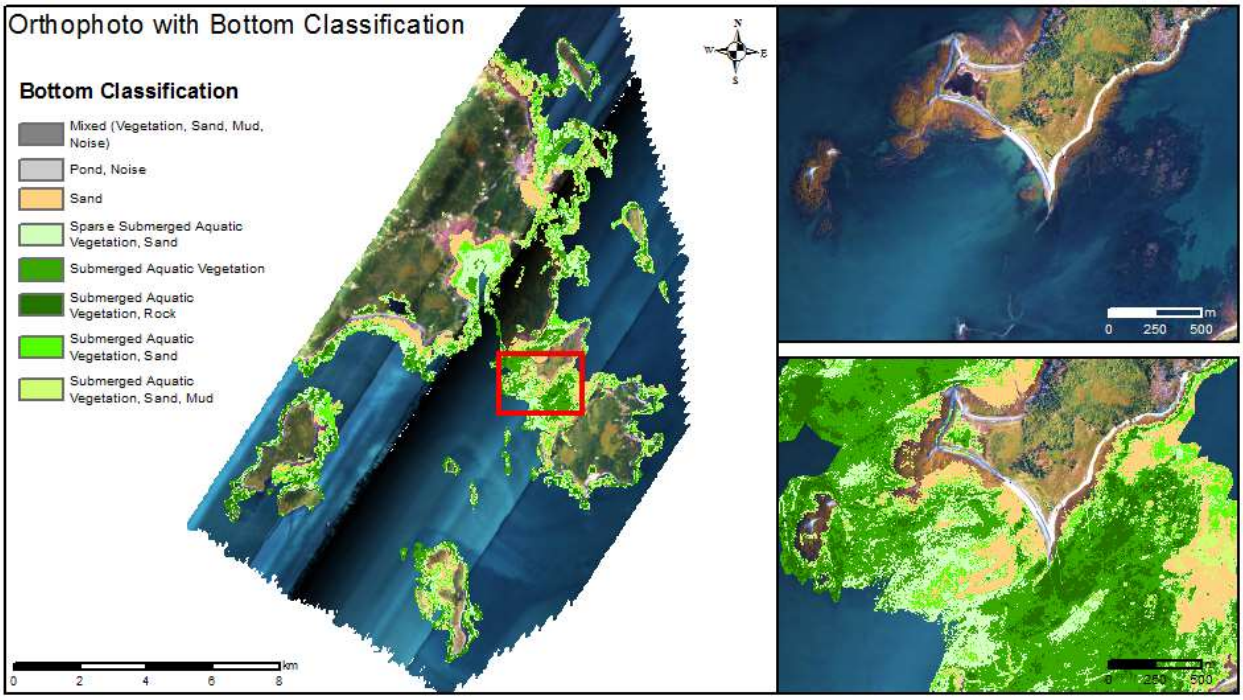


**Figure 3.33: Grand Manan bottom classification with orthophoto mosaic.**

| Value | Bottom Type |
|---|---|
| 1 | Pond; Noise |
| 2 | Submerged Aquatic Vegetation; Rock |
| 3 | Submerged Aquatic Vegetation |
| 4 | Sparse Submerged Aquatic Vegetation; Sand |
| 5 | Submerged Aquatic Vegetation; Sand |
| 6 | Sand |
| 7 | Submerged Aquatic Vegetation; Sand; Mud |
| 8 | Mixed (Vegetation, Sand, Mud, Noise) |

**Table 3.3: Classes used in Grand Manan bottom classification.**

Figure 3.34 highlights the results of the SAV map for Grand Manan. Comparable to the results of the bottom classification, there is a large amount of submerged aquatic vegetation dispersed throughout the study area. It is also possible to see where the sand along the coastline due to the absence of vegetation.

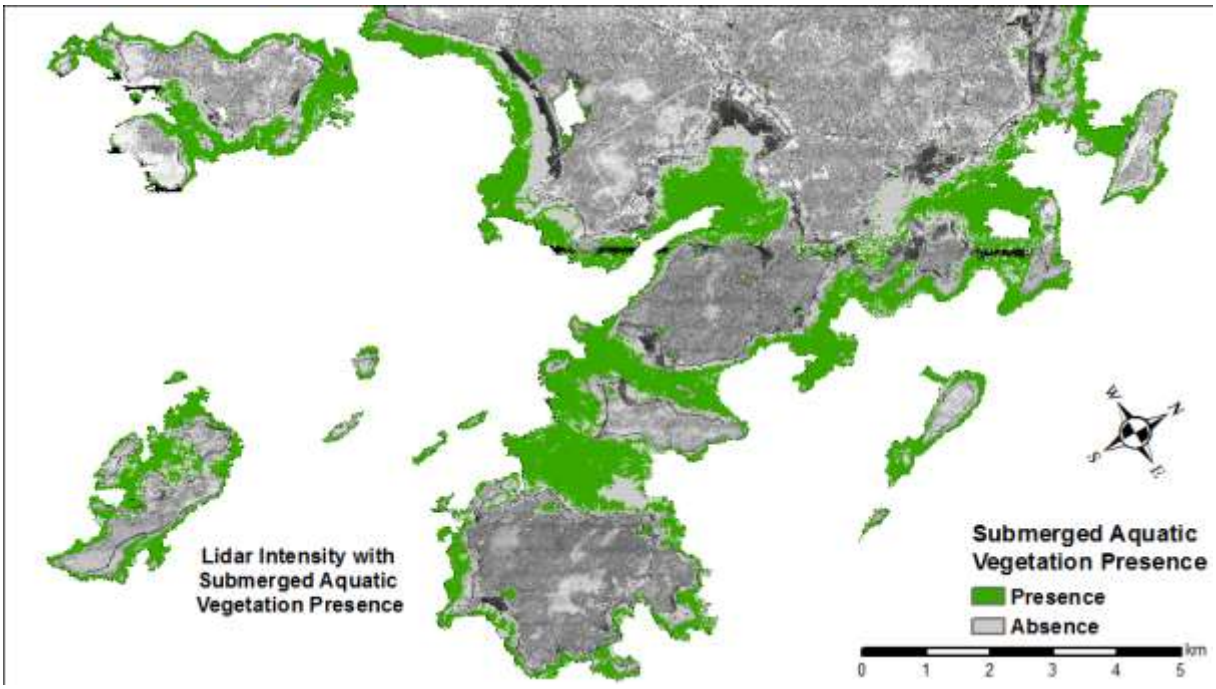


**Figure 3.34: Grand Manan submerged aquatic vegetation map showing presence of vegetation in green and absence in grey.**

## 3.5 Shoreline Classification Results

### 3.5.1 Grand Manan

Figure 3.35 presents the shoreline classification extent for southeastern Grand Manan Island. This classification combines the day 1 and 2 survey flights. The results of the shoreline classification indicate that the shoreline is composed primarily of vegetated bank with sand beach (Figure 3.36). Additionally, there is pebble/cobble beach and boulder beach along the shoreline as pictured in Figure 3.37. Figure 3.38 presents similar results, highlighting an area containing the pebble and cobble noted above, as well as vegetated bank. The colours used in the shoreline classification are Environment Canada standard and the image shown on the map is the orthophoto mosaic derived from the lidar survey.

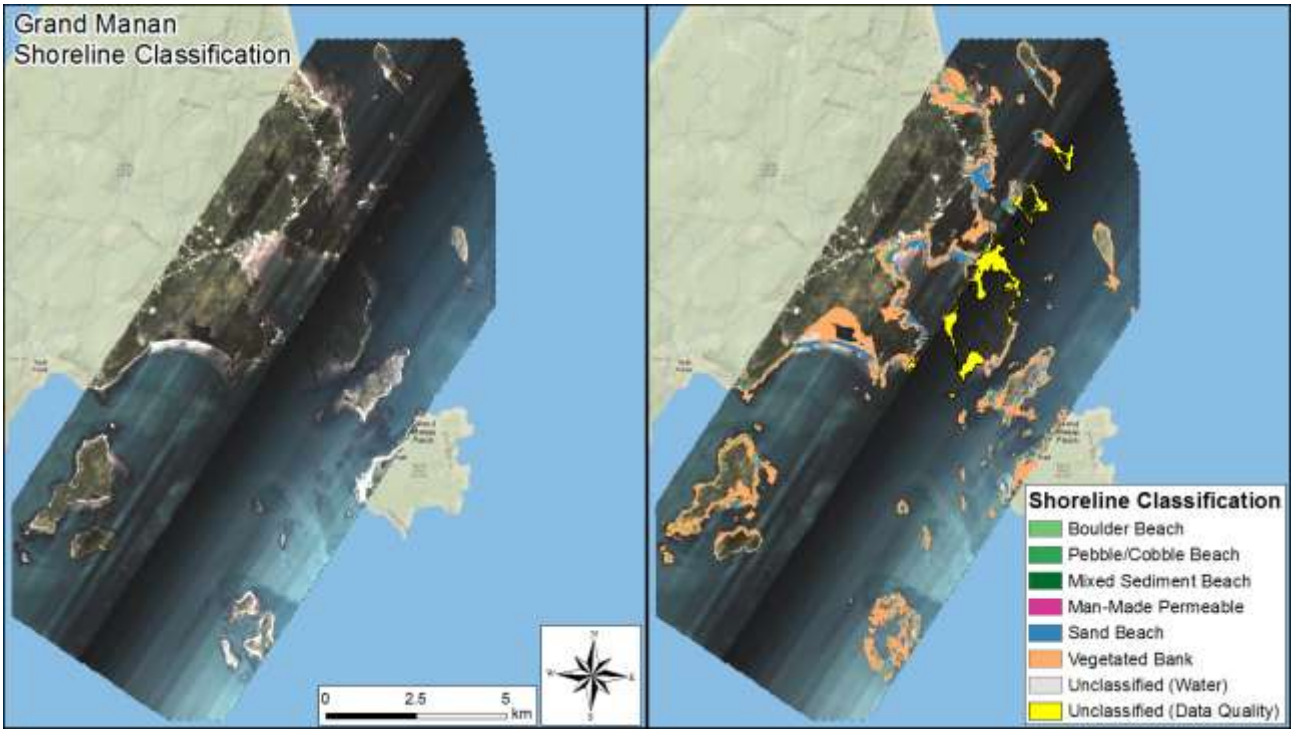


**Figure 3.35: Shoreline classification of Grand Manan for the day 1 and day 2 flights combined. Shown is the orthophoto mosaic.**


**Figure 3.36: Shoreline classification of Grand Manan for the day 1 and day 2 flights combined and zoomed to highlight beach area. Shown is the orthophoto mosaic.**

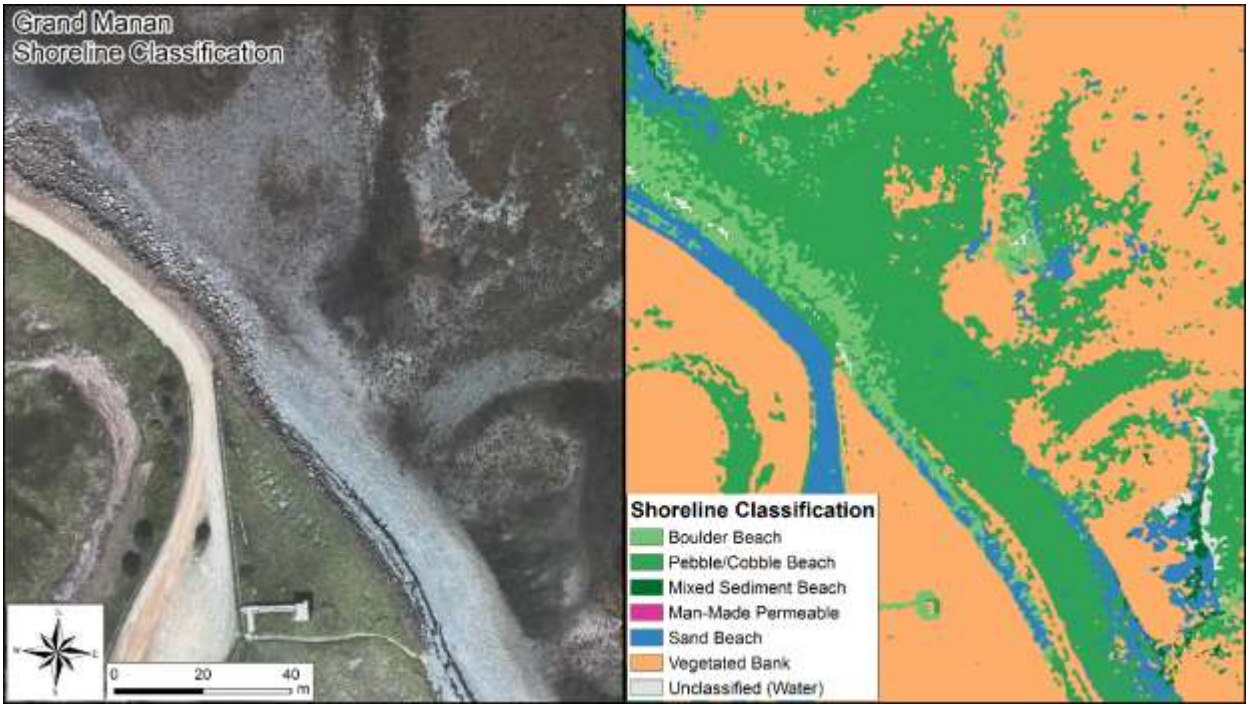


**Figure 3.37: Shoreline classification of Grand Manan for the day 1 and day 2 flights combined and zoomed to highlight nearshore area. Shown is the orthophoto mosaic.**

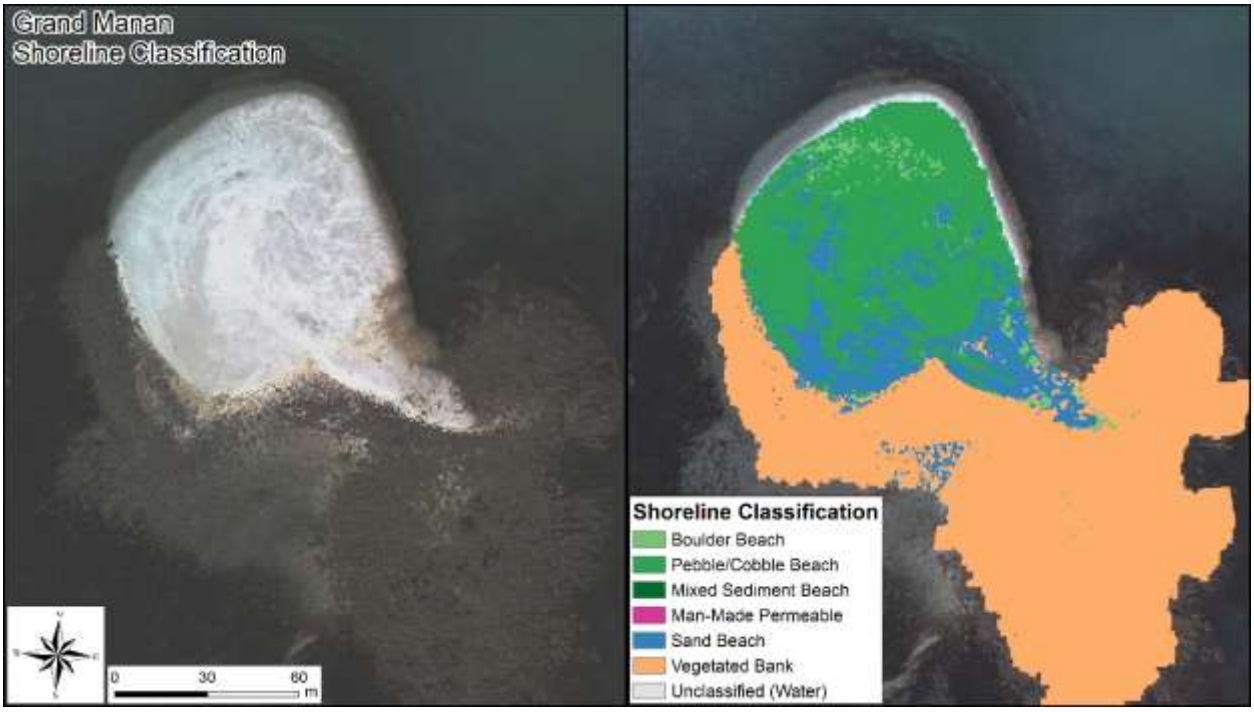


**Figure 3.38: Shoreline classification of Grand Manan for the day 1 and day 2 flights combined and zoomed to highlight submerged area. Shown is the orthophoto mosaic.**

# 4 Discussion/Conclusions

Airborne topographic-bathymetric lidar surveys flown in 2016 for the four Tanker Safety areas were successful in penetrating the majority of the sea bed: in Big Basin, the lidar reached minimum elevation values of -4.94 m CGVD28 (~ MSL), however, it was not successful in penetrating to the center of the Basin due to deep bathymetry and poor water clarity; in Canso, minimum elevation values were -14.91 m CGVD28; in Deer Island, minimum elevation values were -13.17 m CGVD28; and in Grand Manan, minimum elevation values were -11.35 m CGVD28. The lidar data was validated using both the topographic and bathymetric RTK GPS (where applicable), as part of standard AGRG analysis. In Grand Manan, there were 1216 points collected along the roads and wharves within the study area with a calculated mean ΔZ of -0.1 m ± 0.02 m. In Canso, there were 3718 points collected along the roads within the study area with a calculated mean ΔZ of -0.04 m ± 0.04 m. For the bathymetric validation results, in Canso, there were 11 direct seabed elevation measurements with a calculated mean ΔZ of -0.09 m ± 0.2 m.

Hydrodynamic (HD) models were developed for Canso and Isle Madame to model circulation into the regions from the Chedabucto Bay and provide examples of travel time of spilled contaminants and near-shore current speeds to assist with cleanup strategies.

Ground truth data collected by AGRG was helpful in determining water clarity, bottom type, and the distribution of vegetation. These data were presented on maps overlaid with the orthophoto mosaics. Overall, the maps illustrated a cover type of mainly mud and some eelgrass in Big Basin. In Canso, the cover type was mainly sand with eelgrass and fucus. Water clarity was an issue in Big Basin, particularly in the center of the Basin, which is consistent with the results of the lidar survey.

Bottom classification maps were produced for Big Basin, Canso, and Grand Manan. SAV maps were also derived. The bottom classification for Big Basin resulted in a primary cover type of submerged aquatic vegetation and submerged aquatic vegetation; sand. In Canso, the primary cover type consisted of vegetation, specifically kelp, moss, and seaweed. Additionally, there was a large amount of deep sand/mud in the northern areas of Canso. In Big Basin and Canso, the classification results were compared to the AGRG ground truth bottom type to compare the results. Overall, the agreement was consistent in both areas. In Grand Manan, the bottom classification resulted in a primary cover type of submerged aquatic vegetation.

A shoreline classification map was produced for Grand Manan. The classification resulted in a primary cover type of submerged vegetation and bedrock with dense vegetation. The information on water movement, bottom type, and water depth provided by this project will allow DFO to characterize the estuaries, ensure safe navigation of tankers into the ports, and to better manage response time and logistics.

# 5 References

DHI Water & Environment (2008). MIKE 21 FLOW MODEL HINTS AND RECOMMENDATIONS IN APPLICATIONS WITH SIGNIFICANT FLOODING AND DRYING.

Dupont, F., Hannah, C.G., and Greenberg, D. (2005). Modelling the Sea Level in the Upper Bay of Fundy. Atmos-Ocean *43*, 33–47.

Varma, H., Hannah, C., MacNab, R., Costello, G., Spears, T., Woodford, W., and Delbridge, C. (2008). The Complexities in the Design and Definitions of the North West Atlantic Data Set; Searching for Rational Architecture to Implement Diverse Bathymetric Data. Proc. Can. Hydrogr. Conf. Natl. Surv. Conf.

Webster, T.L., McGuigan, K., Crowell, N., Collins, K., and MacDonald, C. (2016). Optimization of data collection and refinement of post-processing techniques for Maritime Canada's first shallow water topographic-bathymetric lidar survey. J. Coast. Res.

# 6 Acknowledgements

We would like to thank the Department of Fisheries and Oceans for funding support for this project. We would like to thank DFO for ongoing support through this project throughout the earlier phases. Thanks to staff from Leica Geosystems, Leading Edge Geomatics staff for operations and AGRG staff for administrative support and the pilots from Leading Edge Geomatics.